

An Assessment of
Ford 3.4 Liter DOHC V8 SHO
Engine Camshaft Failures

by

Bruce C. Lamartine, Ph.D.

4/27/2004

Copyright © **2004**

by

Bruce C. Lamartine

ABOUT THE AUTHOR

Bruce Lamartine is a Technical Staff Member and Intellectual Property Coordinator at Los Alamos National Laboratory. Prior to that, he was a Technical Staff Member with both the U.S. Air Force Materials Laboratory and Motorola Semiconductor Products Sector. He holds a Ph.D. in Physical Chemistry from Case Western Reserve University. Dr. Lamartine has led successful failure analysis teams for the U.S. Air Force in the fields of pressed metal powders and electronic emissive materials. He has 75 scientific publications, 7 issued US and foreign patents, 1 pending US patent, 3 pending foreign patents, 5 biographical citations, and 12 career awards including the Air Force Commendation Medal. His research has centered on surface chemistry, failure analysis and production plant troubleshooting, and nanoengineered surfaces.

ABSTRACT

Camshaft failure in an interference engine such as that used in the 3.4 liter DOHC V8 engine of the 1996-1999 Ford SHO (also known as the Ford Gen III SHO) could be a potentially lethal event. Sufficient literature indicating premature failure of the drive sprockets existed years before production commenced on the Ford Gen III SHO. From the literature publicly available prior to production, we were able to use both a gear tooth stress model and a valve train resonance model to predict a band of failures remarkably consistent with the camshaft failures actually occurring after production. Available Ford Gen III SHO camshaft failure data were analyzed by nonlinear least squares regression techniques. The most probable camshaft failure mileage was found to occur at approximately 70,000 miles, beyond Ford warranty, but still early in engine life. Consistent with the physics of random impacts and the assumption of the use of St 52 DOM steel tubing in camshaft assembly, the data were best fitted by a single Birnbaum-Saunders distribution function to better than the 95% confidence level usually required by courts of law. It is very unlikely that performance driving alone is responsible for all camshaft sprocket failures; rather, extreme performance driving may account only for the low mileage branch of the observed camshaft failure distribution and then only when very poor force locking and/or high lobe torques also occur. Insufficient spline contact area appears to be the most likely source of sprocket failure, and, given the literature of the time and reasonable engineering expertise, this defect should have been recognized and corrected before production. Lifetime predictions of two failure remedies are also reported.

TABLE OF CONTENTS

INTRODUCTION..... 6

MODELS AND CALCULATIONS..... 7

A Physical Model of Failure..... 8

Miner’s Rule.....14

The Birnbaum-Saunders Distribution 14

The Power Birnbaum-Saunders Approximation 16

A Priori Estimates of Failure..... 18

Method 1: Gear tooth stress limit model 18

Limits of tubing expansion and resultant contact area..... 19

Stresses applied to tubing teeth 20

A model of tool wear..... 20

Method 2: Lobe torque model..... 25

An estimate of applied torque..... 26

The relation of specific energy to applied torque..... 29

Consideration of valve spring resonance forces..... 31

Analysis of the Failure Data..... 35

RESULTS AND DISCUSSION..... 37

Comparison with Failure Models..... 37

A Vulnerability Estimate..... 39

Methods to Extend Drive Sprocket Life..... 39

CONCLUSIONS AND RECOMMENDATIONS..... 42

ACKNOWLEDGMENT..... 43

REFERENCES..... 44

INTRODUCTION

Due to the interference design of the 3.4-liter DOHC V8 SHO engine, a camshaft sprocket failure usually leads to additional damage to valves, pistons, and other major engine parts. Such a failure often leads to loss of vehicle control since power steering and power brakes are also lost when the engine fails. At this writing, we are thankfully unaware of any associated fatalities. A typical repair bill is around \$6000, and a new engine can cost as much as \$15,000. A complaint has been filed against Ford Motor Company [1] alleging that Ford had knowledge of the camshaft sprocket product defect early in the product cycle. It is the intent of this paper to show that engineering literature available to Ford and the public at large well before the time of manufacture strongly suggested that the sprocket of an assembled camshaft was a likely point of failure; and furthermore, that the failures were to be expected at the mileages later publicly reported. This paper will also show that corrective measures already known by at least as early as 1992 could have been implemented either before or during the time of manufacture to avoid this product defect.

Since early 2000 at least, an association of Gen III Ford SHO owners (V8SHO.com) has recorded the camshaft sprocket failures of their members [2]. As of mid-April 2004, some 385 sprocket failures (approximately 295 with mileages at failure) have been publicly documented by this organization. While internal Ford records of these failures would most likely be a larger data sample, the public data are nevertheless a sufficiently large sample to recover significant information. We have chosen to follow the analysis practices set forth by the National Institute of Standards and Technology (NIST) known as Exploratory Data Analysis (EDA). EDA is a combination of graphical and numerical techniques [3]. For court compatibility where appropriate, we have also included the conventional chi-square statistical tests at the 95% confidence level [3,4].

Crucial to further analysis is the assumption of the actual species of steel tubing used, and we have made speculations only. Ford, however, is known to have used an assembled camshaft on the Mondeo, a V6 European model [5]. The supplier for that engine was identified as Thyssen-Krupp Presta. No particular grade of steel tubing was revealed in that reference; but we do know from public import relief request documents [6] that only 26Mn5 and St52 (both DIN 2393 grade) were specified as the highest European standard for drawn over mandrel (DOM) tubing intended for use in assembled camshaft manufacture. St52 is a low carbon steel of high yield strength and well-known strain-life properties [7].

Regardless of the actual assembly process used, the steel tubing is deformed to form features which engage the camshaft elements such as drive sprockets, bearing sleeves, and cam lobes. The patent literature prior to 1995 points out a number of limitations of this kind of manufacturing, particularly the potential weakness of drive sprockets, although no quantitative physical arguments appeared. An assembled camshaft patent [11] issued in 1992 and assigned to the company Emitec in Germany specifies St35 (an

older, weaker steel composition) or St52 as the tubing used in the preferred embodiments. A second patent (issued in 1991) also assigned to Emitec [12] specifically points out the potential for failure at the drive sprocket. There are similarities between the drawings in the Emitec patents and the pictures shown on the member website [2]. Essential differences, however, are the internal spline design for the drive sprocket and the internal deformation pattern. It is here that the contact area is obtained upon tubing expansion (see below). An assembled camshaft and its method of manufacture wherein a star-shaped mandrel is used for internal plastic expansion was patented by Bendoraitas and Clark [13,14] in 1989. The patent was assigned to the Torrington Company. The internal expansion of the Gen III Ford SHO camshaft shows evidence of the use of a star mandrel or similar device. Consequently, it appears likely to this author that Thyssen-Krupp Presta was the supplier of camshafts for 3.4-liter DOHC V8 SHO engines and that some variation of the Emitec or Torrington assembly process was used.

The methods of assembling camshafts were also well reported in the patent literature of the late 1980s and early 1990s. All assemblies of the time appear to have been made in an elaborate jig where all lobes and sprockets are aligned before force locking. Force locking is achieved by either hydraulic expansion of selected tubing regions [11], ballizing; i.e., forcing an extremely hard oversize metal ball (usually tungsten carbide) down the inside of the camshaft tubing [15,16], or splined mandrel expansion where a forming device is passed through the inside of the tubing [13,14]. As a result of any of these methods of manufacture, the tubing sees internal pressures in the range of 2000-3500 bar (200-350 MPa) [11] and deforms plastically into the groove region between the element (sprocket, bearing sleeve, or lobe) splines. Expansion of the outer diameter of the tubing in this region is typically no more than 10-15% of the tubing thickness [11]. This means that the depth of the element must be designed appropriately in order to produce a contact area sufficiently large so that the stress applied on the tubing is low enough that the strain produced insures sufficiently long service life. It should be noted that a service life on the order of 100 million-10 billion reversals is sought and that early fatigue designs for steels assumed infinite life beyond approximately 1 million reversals [17]. Even more recent strain-life models can overestimate the lifetime if insufficient data (or an insufficient data interval) is taken in the high fatigue cycle range.

MODELS AND CALCULATIONS

A table of approximately 1200 data pairs was generated for each equation in order that its graph could be presented with an equivalent resolution of ± 590 miles at 70,000 miles. At least five significant figures were carried through all exponential and logarithmic calculations. Common software packages available today for such work are Mathematica, Matlab, and Mathcad. Mathcad was chosen for this work because tabular data corresponding to a single graphical point could be extracted by the "trace" function. Similar operations using a lookup table could have been programmed with ease by workers in the late 1980s using the FORTRAN and BASIC computing environments. BASIC software of the time also had an internal graphics package sufficient for this work.

A physical model of failure.

We treat our expanded tube as if it were a gear with individual teeth that mesh with the camshaft element splines and fail in the manner of cantilevered beams. Fig. 1a shows an actual cross-section of a Gen III camshaft drive sprocket [2] and Figs. 1b-d show the conceptual detail of the complementary tubing expansion region.



Figure 1a. A section of a failed Gen III camshaft drive sprocket. Photo by Bob Gervais. Downloaded from [2] with webmaster permission.

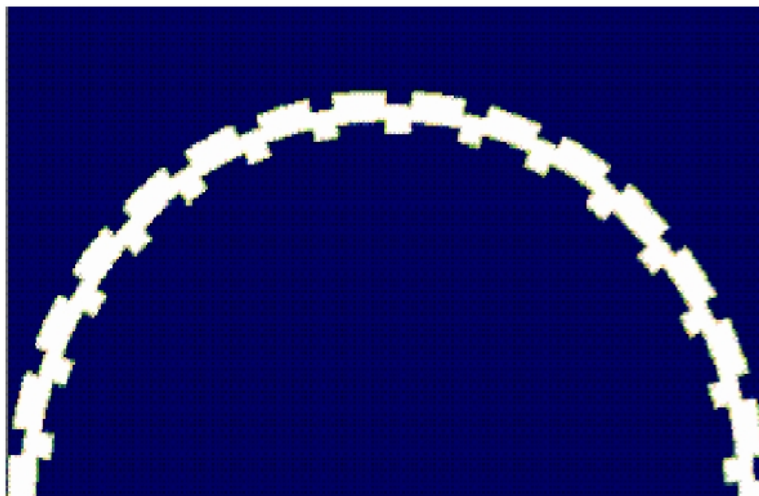
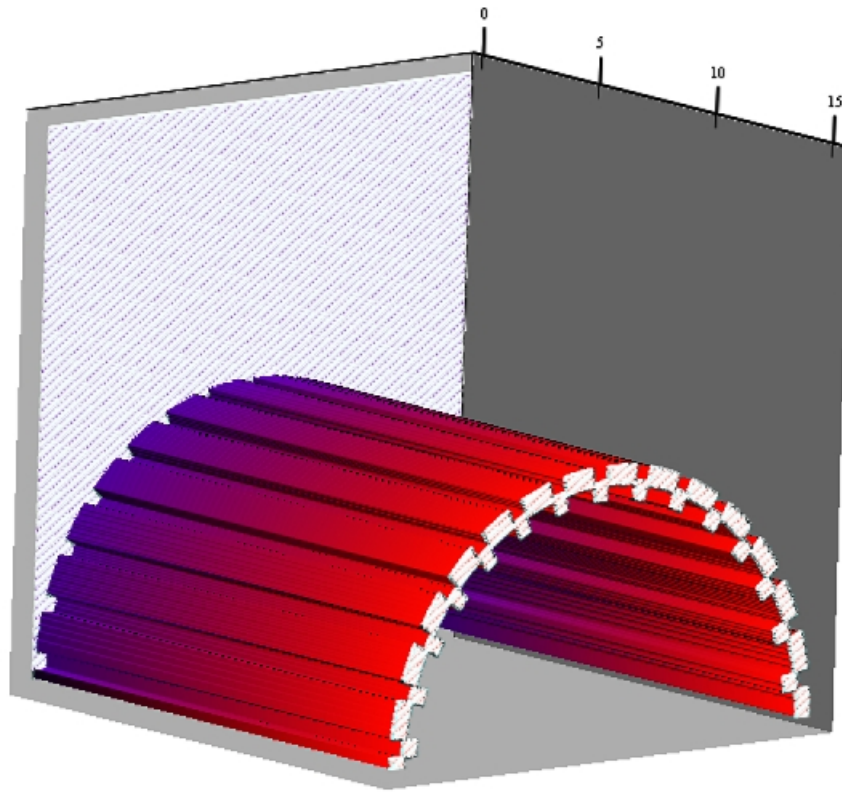


Figure 1b. Cross-sectional model of Gen III camshaft tubing after force locking by star mandrel to the drive sprocket. The outer splined edge of this tubing meshes with the concave grooved region of the sprocket shown above in Fig. 1a. The radial expansion was exaggerated in this calculation for clarity [18].



U

Figure 1c. Three-dimensional model of Gen III camshaft tubing after force locking by star mandrel to the drive sprocket. The outer splined edge of this tubing meshes with the concave grooved region of the sprocket shown above in Fig. 1a. The radial expansion was exaggerated in this calculation for clarity [18].

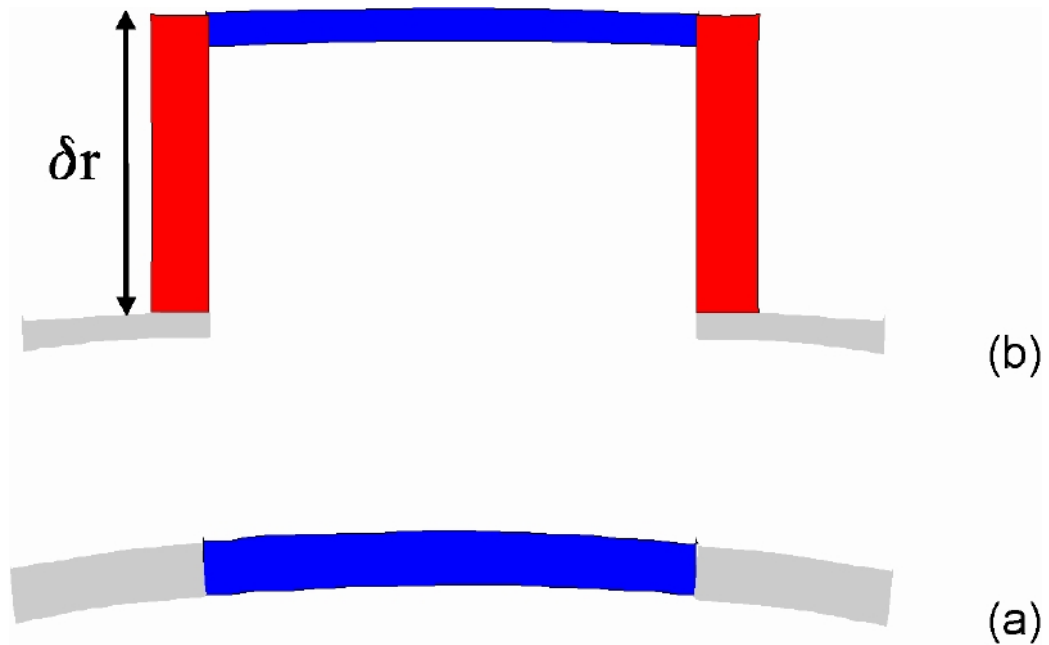


Figure 1d. Detail of force locking tubing expansion. (a): Before expansion. (b): After expansion. The radial displacement δr is **exaggerated for clarity**. **Although movement of material is shown, conservation of volume is assumed (see Method 2 below).**

Several models of gear tooth stress are available [19-21], but the simplest of these (available in 1981 [19]) suffices for further analysis if the ultimate strength and the elastic limit of the tubing material are known. Fortunately, the entire stress-strain curve for St52 steel was known at least as early as 1972 [22], and we have digitized data from that source for further use in lifetime prediction. It should be noted that the slope of the elastic region of the stress-strain curve is almost invariant with temperature. Thus we have confidence that a low-temperature curve will suffice to describe small camshaft element stresses at all operating temperatures. Fig. 2 shows the stress-strain curve used.

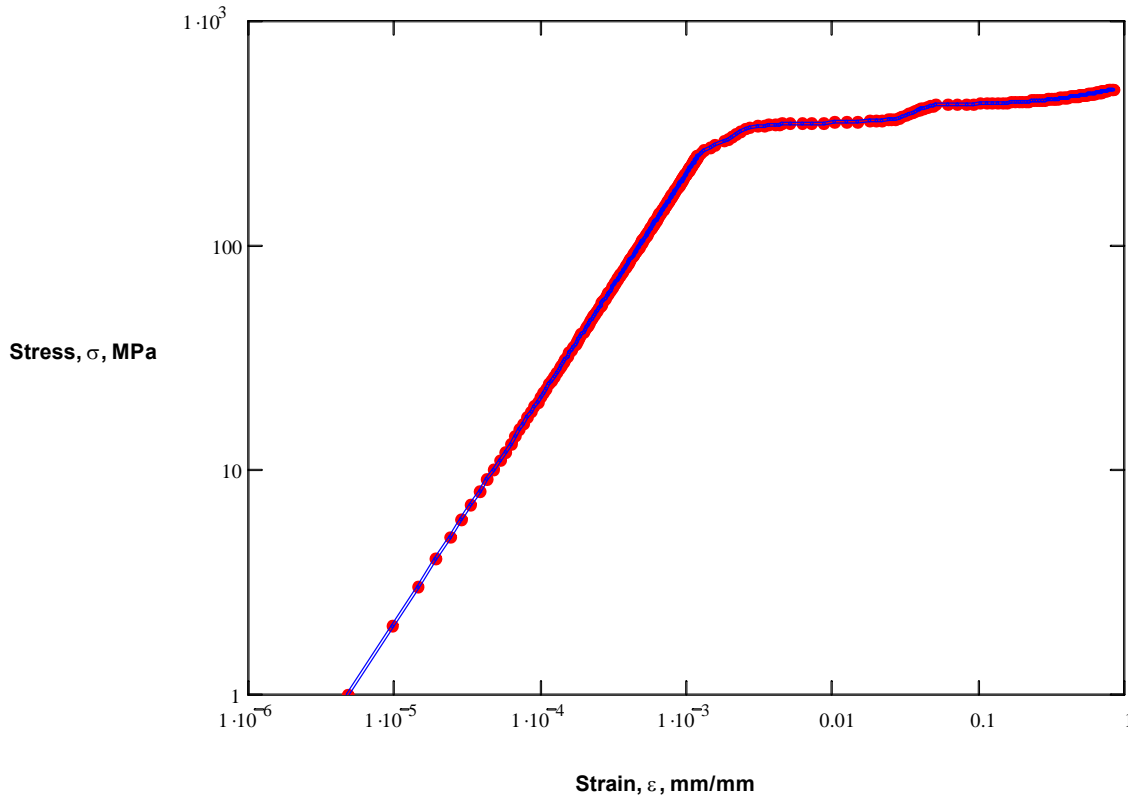


Figure 2. Data digitized from the stress-strain curve of St52 steel at 20 degrees C [22]. Note the logarithmic axes.

The strain-life of metals was investigated systematically in the early 1970s [23], and four parameter strain-life coefficients of St52 steel can be derived from the data reported at least as early as 1987 [7]. A strain-life equation for the total strain ε is

$$\varepsilon \equiv \frac{\sigma_f}{E} \cdot (2 \cdot N_f)^b + \varepsilon_f \cdot (2 \cdot N_f)^c, \quad (1)$$

where σ_f , b , ε_f , c , E , and N_f are the fatigue strength coefficient, the fatigue strength exponent, the fatigue ductility coefficient, the fatigue ductility exponent, Young's modulus, and the number of fatigue cycles, respectively. The data presented in [7] show evidence of an endurance limit typical of triangular load waves of constant amplitude and frequency. In a camshaft application, however, random load amplitudes and frequencies are applied; and consequently, a continually decreasing strain as a function of life rather than an endurance limit is expected [8]. A more appropriate representation of high cycle fatigue in this case is obtained when the coefficients of the strain-life equation are

calculated from single frequency test data representing both low and high cycle fatigue (beyond transition life) but not including noisy data typical of an endurance limit. Figure 3 shows the combined data for duplicate runs of St52 steel as well as the strain-life curves calculated [9] for single frequency and random frequency loading. The random frequency case compares well to a later curve, also shown in Fig. 3, given by Ilzhofer, et al. [10] for multiple frequency impacts on a moment loaded round bar. The coefficients,

$$\begin{pmatrix} \sigma_f \\ b \\ \varepsilon_f \\ c \\ E \end{pmatrix} := \begin{pmatrix} 1.43 \times 10^3 \\ -0.136 \\ 0.967 \\ -0.646 \\ 210000 \end{pmatrix},$$

obtained from a four parameter fit of that St52 strain-life curve, were used in all subsequent calculations in this work.

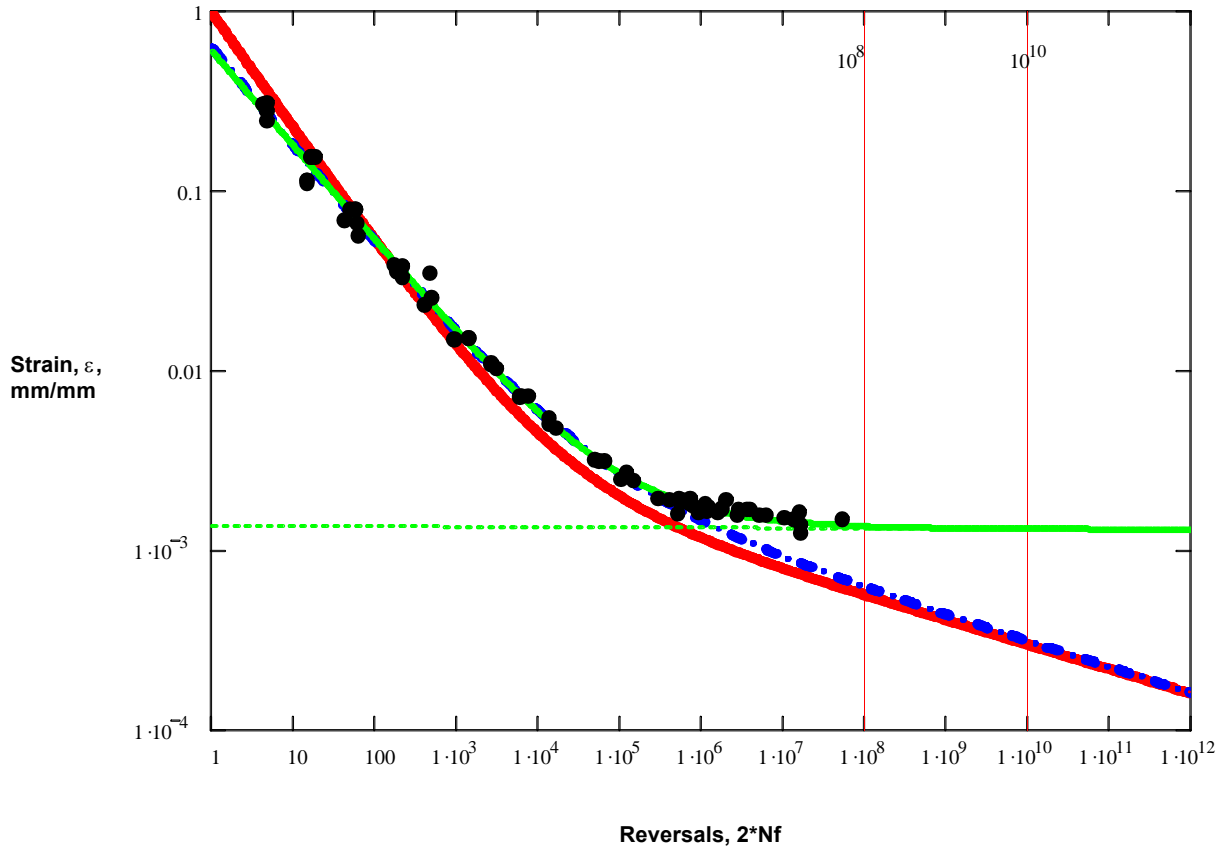


Figure 3. Strain-life data of St52 steel having $E = 210,000$ MPa from [7] and fitted curves: Black dots, data from single frequency loading; Green solid line, fitted to endurance limit; Blue dash-dot, fitted neglecting endurance limit; Red solid line, a strain-life curve of St 52 with multiple frequency loading calculated with coefficients derived from [10]. The camshaft sprocket failure range of $10^8 - 10^{10}$ reversals is also shown.

In the elastic range of strain-life (high numbers of stress reversals), the fatigue curve can be approximated by

$$\varepsilon_e = \frac{\sigma_f}{E} \cdot (2 \cdot Nf)^b \quad (2)$$

When used with a simple model of gear tooth stress failure, knowledge of both stress-strain and strain-life are sufficient to estimate the most probable number of reversals to

failure; and if a conversion from the number of reversals to mileage can be made, a most probable failure mileage can be calculated. In the case of the expanded force-locked tubing, the radial expansion is an additional variable that can be used to estimate upper and lower limits of the failure mileage.

Materials failures due to fatigue are usually characterized by either a lognormal or a Birnbaum-Saunders distribution (first reported in 1969 [24]), depending upon the assumed influence of prior load history. In either distribution, a lower limit, most probable value, and upper limit are sufficient to estimate the entire failure distribution and its associated probability density. We argue below for a failure model that uses the Birnbaum-Saunders distribution.

Miner's Rule.

In order to discover a failure distribution, we must first find a physical basis for a failure model. If we assume that each cam lobe impact force is independent of influence from previous impacts and is counteracted by an equal but opposite force on the drive sprocket splines, then those splines accumulate a sum of individual stresses Y where each applied stress has its own expectation, m , and variance, σ^2 ; i.e., the crack growth that occurs in any one strain cycle is independent of that in any other cycle. Miner's rule states that the damage that occurs after n cycles, at a stress that produces failure at N cycles is proportional to n/N .

The Birnbaum-Saunders Distribution.

We further assume that, at failure in many samples, the sum of the individual stresses Y will be distributed around some critical number of stresses w . We seek the probability that n will be greater than w ; and since n and w are large, we use the Central Limit Theorem [25,26] to produce a reduced variable T :

$$T = \frac{m\sqrt{n}}{\sigma} - \frac{w}{\sigma\sqrt{n}} \quad (3)$$

Substitution of

$$\sigma = c\sqrt{2}, \quad w = \sqrt{\mu}, \quad \text{and} \quad m = \frac{1}{\sqrt{\mu}},$$

where μ is the median and c is a shape parameter leads to

$$T = \frac{1}{c\sqrt{2}} \cdot \left[\left(\frac{n}{\mu} \right)^{\frac{1}{2}} - \left(\frac{n}{\mu} \right)^{\frac{-1}{2}} \right] \quad (4)$$

According to the Central Limit Theorem, the distribution of failures is then a Gaussian function of T :

$$\Phi = \frac{1}{2} \cdot \left[1 + \operatorname{erf} \left[\frac{1}{c \cdot \sqrt{2}} \cdot \left[\left(\frac{n}{\mu} \right)^{\frac{1}{2}} - \left(\frac{n}{\mu} \right)^{\frac{-1}{2}} \right] \right] \right] \quad (5)$$

The form above is known as the Birnbaum-Saunders cumulative probability density function (cdf). Its derivative or probability density function (pdf) [27,28] is

$$\phi = \frac{1}{2 \cdot \sqrt{2 \cdot \pi} \cdot c \cdot \mu} \cdot \left[\left(\frac{n}{\mu} \right)^{\frac{-1}{2}} + \left(\frac{n}{\mu} \right)^{\frac{-3}{2}} \right] \cdot \exp \left[\frac{-1}{2 \cdot c^2} \cdot \left[\left(\frac{n}{\mu} \right)^{\frac{1}{2}} - \left(\frac{n}{\mu} \right)^{\frac{-1}{2}} \right]^2 \right] \quad (6)$$

If g (the most probable value of ϕ) can be found, sufficient information to estimate the entire failure distribution (or its pdf) would then be known. The exact solution for g can be found either by solving equation (6) for its maximum (this is usually done numerically) or by solving the analytical derivative of equation (6) for its zero crossing. Alternatively, a very good approximation for g can be derived as shown below.

The Power Birnbaum-Saunders Approximation.

The Birnbaum-Saunders distribution described above is in fact a specific case of the generalized Power Birnbaum-Saunders distribution [27] which can be written in the cdf form

$$Q = \frac{1}{2} \cdot \left[1 + \operatorname{erf} \left[\frac{\left(\frac{n}{\mu} \right)^{\frac{\lambda}{2}} - \left(\frac{n}{\mu} \right)^{\frac{-\lambda}{2}}}{c \cdot \lambda \cdot \sqrt{2}} \right] \right], \quad (7)$$

where

$$0 < c < \infty \quad , \quad 0 < \lambda < \infty \quad , \quad \text{and} \quad 0 < n < \infty \quad ,$$

or otherwise in the pdf form

$$q = \frac{1}{2 \cdot \sqrt{2 \cdot \pi} \cdot c \cdot \mu} \cdot \left[\left(\frac{n}{\mu} \right)^{\frac{\lambda}{2}} + \left(\frac{n}{\mu} \right)^{\frac{-\lambda}{2}} \right] \cdot \left[\left(\frac{n}{\mu} \right)^{-1} \right] \cdot \exp \left[\frac{-1}{2 \cdot c^2 \cdot \lambda^2} \cdot \left[\left(\frac{n}{\mu} \right)^{\frac{\lambda}{2}} - \left(\frac{n}{\mu} \right)^{\frac{-\lambda}{2}} \right]^2 \right], \quad (8)$$

where

$\lambda > 1$ is the Power Birnbaum-Saunders distribution,
 $\lambda = 1$ is the Birnbaum-Saunders distribution, and

$\lim_{\lambda \rightarrow 0} q$
 $\lambda \rightarrow 0$ is the pdf of the lognormal distribution, namely

$$\kappa = \frac{1}{\sqrt{2 \cdot \pi} \cdot c \cdot \mu} \cdot \left(\frac{n}{\mu} \right)^{-1} \cdot \exp \left[\frac{-1}{2 \cdot c^2} \cdot \left(\ln \left(\frac{n}{\mu} \right) \right)^2 \right]. \quad (9)$$

Several Power Birnbaum-Saunders pdfs with arbitrary values of λ are shown in Fig. 4.

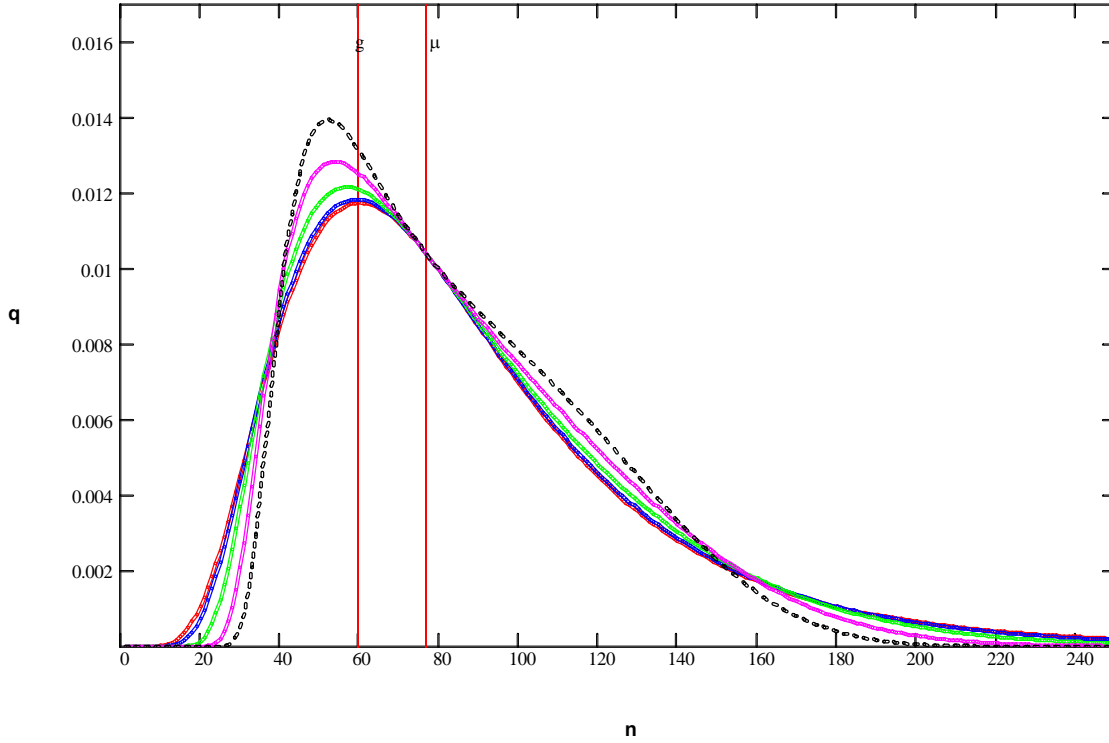


Figure 4. The Power Birnbaum-Saunders distribution pdf (at $\mu=77$ and $c=0.5$) for several values of λ as given in eq. 8: red, $\lambda = 0.00001$; blue, $\lambda = 1$; green, $\lambda = 2$; magenta, $\lambda = 3$; and dashed black, $\lambda = 4$. The most probable value of q as λ approaches 0 is given by the term g . The common median μ is also shown.

We can now solve for g by setting the derivative of κ with respect to n equal to zero:

$$\frac{d}{dn} \kappa = \frac{-1}{c \cdot n^2 \cdot \sqrt{2 \cdot \pi}} \cdot \exp\left(\frac{-1}{2 \cdot c^2} \cdot \ln\left(\frac{n}{\mu}\right)^2\right) - \frac{1}{c^3 \cdot n^2 \cdot \sqrt{2 \cdot \pi}} \cdot \ln\left(\frac{n}{\mu}\right) \cdot \exp\left(\frac{-1}{2 \cdot c^2} \cdot \ln\left(\frac{n}{\mu}\right)^2\right); (10)$$

and consequently,

$$g = \frac{\mu}{\exp(c^2)} \quad (11)$$

For

$$c \leq 0.5 \text{ and } \lambda \leq 1,$$

the error of the approximation is less than 1.3%.

A Priori Estimates of Failure.

Method 1: Gear tooth stress limit model.

A common procedure in materials physics is to construct a stress-life curve from stress-strain and strain-life curves. In this manner, design stress and useful life are directly related. This is equivalent to writing the stress σ as

$$\sigma = \sigma(\varepsilon),$$

and the strain ε as

$$\varepsilon = \varepsilon(Nf)$$

so that

$$\sigma = \sigma(\varepsilon(Nf)).$$

We can report the stress life as a function of actual miles driven if a suitable conversion is known. If we assume that all the miles traveled are in overdrive (4th gear) and the final drive ratio is 28.4 mi/hr/1000 rpm [29], then, for a 4 valve/cylinder 4-stroke DOHC V8 engine with simultaneous valve pair action in each cylinder, the conversion is

$$2 \cdot Nf \cdot \left(\frac{2}{8451} \right) = 1 \cdot \text{mile} \quad (12)$$

where Nf is the number of impact cycles applied to the cam lobe by the valve spring. Figure 5 shows a graphical composite calculation for St52 steel which includes the elastic fatigue approximation for failure mileage.

A common European standard (published in 1981) for the stress limit σ_{bw} on gear teeth such as those in our expanded force-locked tubing is [19]

$$\frac{\sigma_{bw}}{\max(\sigma)} = 0.2 \quad (13)$$

This means that

$$\sigma_{bw} = 101.5 \text{ MPa}$$

Using the tie lines shown in Fig. 5, we find that the most probable failure mileage is indicated at 69,843 miles. This number agrees closely with the elastic fatigue approximation (asymptotic limit shown in Fig. 5) of 66,442 miles.

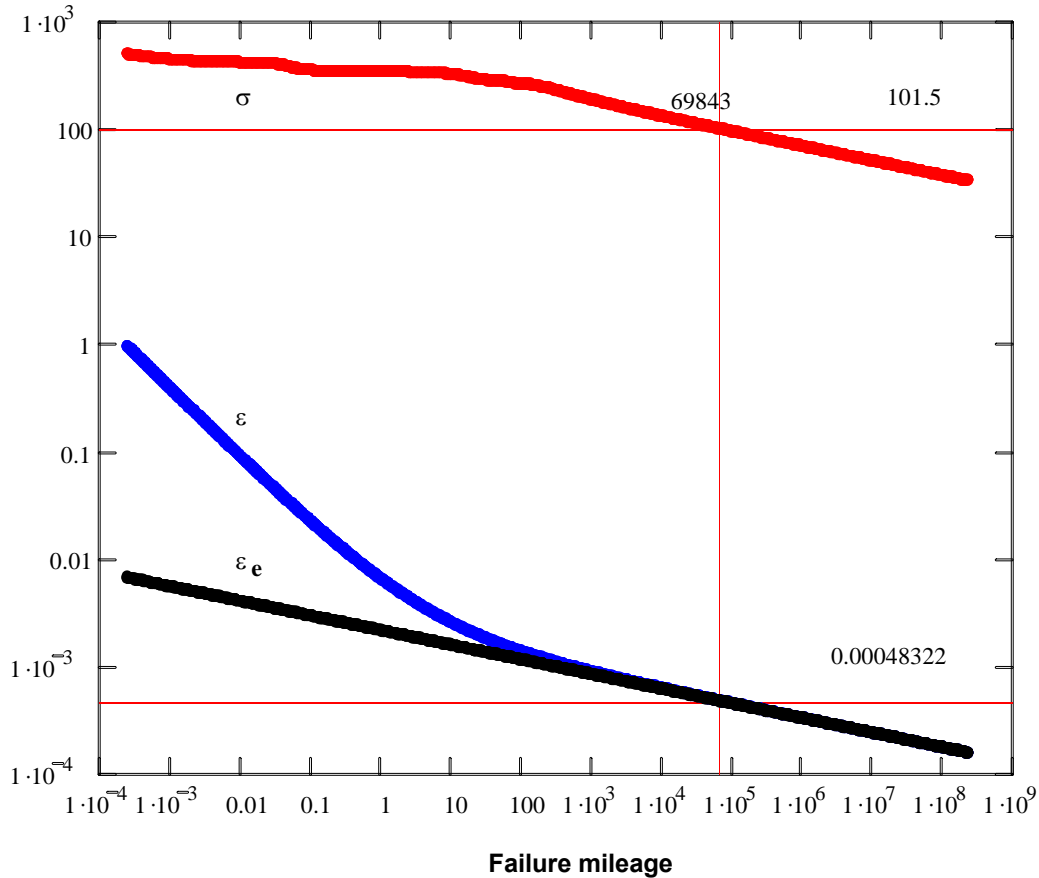


Figure 5. Stress-life curve (red) calculated from the total strain-life curve for St52 steel (blue). The asymptotic elastic strain-life approximation (see eq. 2) is shown in black. For a gear tooth stress limit of 101.5 MPa, a limiting strain of 0.00048322 mm/mm and an associated failure mileage of 69843 miles are estimated.

Limits of tubing expansion and resultant contact area.

The Breuer patent teaches that, for ductile steel tubing, the expected radial expansion during the force-locking process is between 10 to 15% of the wall thickness [11]. In addition, typical variations in wall thickness from a supplier are 40 microns [30,31]. For

a one mm thick wall similar to that used in the V8 SHO camshafts, the expected radial expansion is therefore only 96-156 microns (approximately 0.004-0.006 inches).

Hamilton [32] has recently reported the spline depth (15.24 mm or 0.600 inches) and a number of splines (30) for the V8 SHO camshaft drive sprocket shown in Fig. 1. We have sufficient data, therefore, to calculate the contact area, A, due to a single stress reversal:

$$A = \delta r * n_{splines} * d , \quad (14)$$

where

$$\begin{aligned} \delta r &= \text{tubing radial expansion,} \\ n_{splines} &= \# \text{ of sprocket splines,} \\ &\text{and} \\ d &= \text{sprocket thickness or depth.} \end{aligned}$$

Stresses applied to tubing teeth.

Recalling that stress is actually a measure of applied pressure, we can, by definition, write the equation for maximum gear tooth stress as

$$\sigma_{bw} = \frac{f_{bw}}{A} , \quad (15)$$

where f_{bw} is the applied tangential force associated with the high-cycle fatigue of the gear tooth.

A Model of tool wear.

The radial expansion, δr , is known to be a scalar of the applied pressure [11]. If the contact area of the mandrel, ball, or partitioned hydraulic region is constant, then the expansion is actually proportional to the internal force f_i applied over some constant area B:

$$\delta r = k_1 \cdot \frac{f_i}{B} . \quad (16)$$

In the first plastic regime of St 52 steel where the applied stress is greater than about 250 MPa, the resulting strain is again roughly proportional to the applied stress, but with a constant of proportionality different from the elastic region (see Fig. 6.).

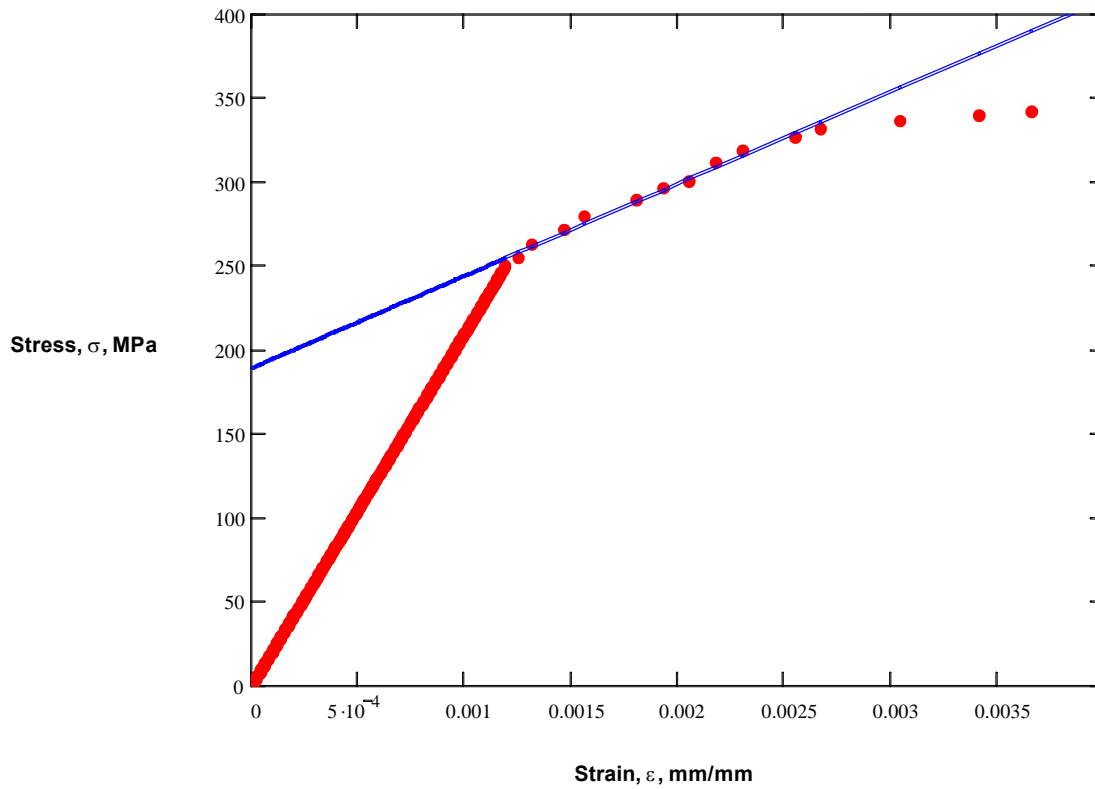


Figure 6. Data digitized from the stress-strain curve of St52 steel at 20 degrees C [22]. The blue line shows approximate linearity in the first plastic deformation region (approximately 250-325 MPa) used to form force locked tubing.

To deform the tubing for force locking, then, the internal force applied is proportional to x , the difference between the tubing ID and the mandrel OD:

$$f_i = k_2 \cdot (x) \tag{17}$$

When the tubing ID remains constant as in our case, x itself becomes proportional to the mandrel radius, r :

$$x = k_3 \cdot (r) \tag{18}$$

Substitution of eqs. 17 and 18 into eq. 16 gives

$$r = \frac{\delta r \cdot B}{k_1 \cdot k_2 \cdot k_3} \quad (19)$$

It is generally accepted that the wear process at constant temperature is of first kinetic order [33]; and consequently, the mandrel wear rate is related to the number of assembly passes η by

$$\frac{d}{d\eta} r = -\beta \cdot (r), \quad (20)$$

where β is a constant. Since we seek a measure of the distribution of δr , we now substitute eq. 19 into eq. 20:

$$\frac{d}{d\eta} (\delta r) \equiv -\beta \cdot (\delta r), \quad (21)$$

whose solution is

$$\eta = \alpha_0 + \alpha_1 \cdot \ln(\delta r), \quad (22)$$

where α_0 and α_1 are constants. The boundary conditions are merely the number of camshafts made (approximately 84,000) and the expansion limits (96 – 156 microns). The normalized cdf of this distribution is shown in Fig. 7. A median expansion value of 112.5 microns was calculated.

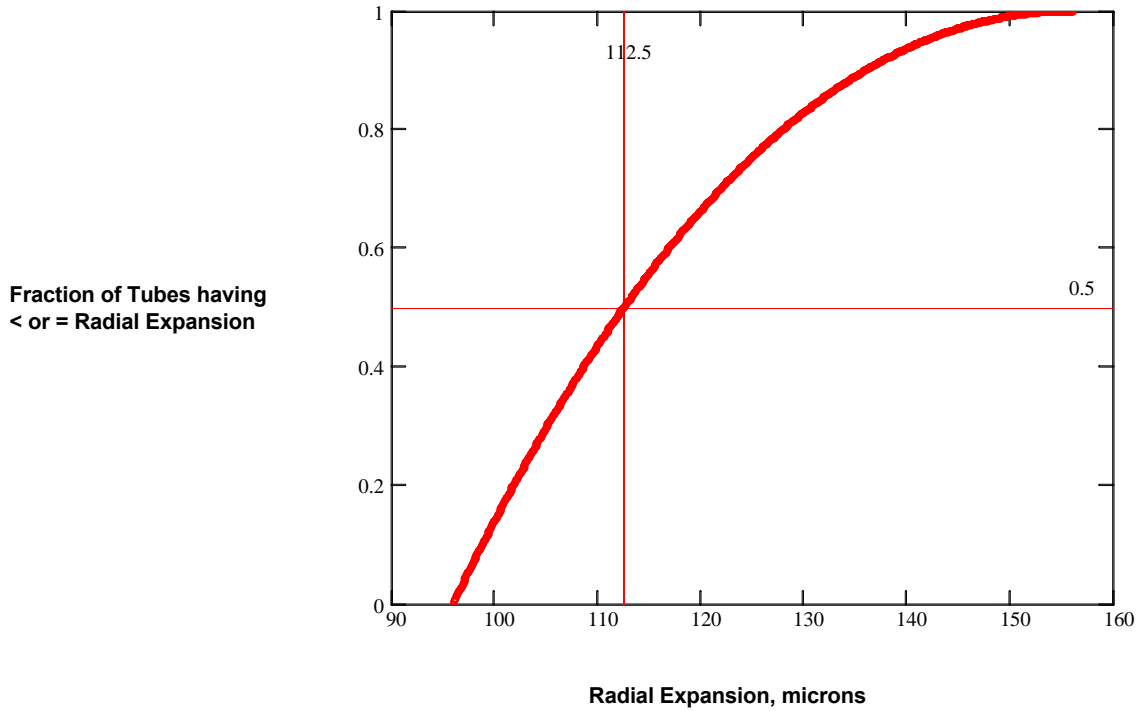


Figure 7. CDF function of eq. 22 showing a median expansion of 112.5 microns.

Solving eq. 15 by substitution of the median δr of 112.5 microns (0.0044 inches) yields an f_{bw} value which was then used in the same equation to estimate high and low values of applied stress. The corresponding values of failure mileage were then read from the graph in Fig. 5 using the Mathcad “trace” function. Values of the variables used are summarized in Table 1 below. These values were also subsequently used to estimate the span of the failure distribution.

Table 1. Values of radial δr , σ , and failure mileage used to estimate the span of the failure distribution estimated by Method 1.

<u>Position</u>	<u>δr, microns</u>	<u>σ, MPa</u>	<u>Mileage</u>
low	96	118.95	22601
most probable	112.5	101.50	69843
high	156	73.20	748380

The low and high failure mileages constitute the estimated limits of the model failure distribution. To a very good approximation, we can construct a band wherein the span of failures constitutes either 6 or 8 standard deviations. The Birnbaum-Saunders constants for these two distributions are given in Table 2 below.

Table 2. Birnbaum-Saunders constants for the failure pdf band of Method 1.

<u>Span, std dev</u>	<u>c</u>	<u>μ, miles</u>
6	0.412	82796
8	0.309	76857

The predicted band of failure lies between the two curves as shown in Fig. 8.

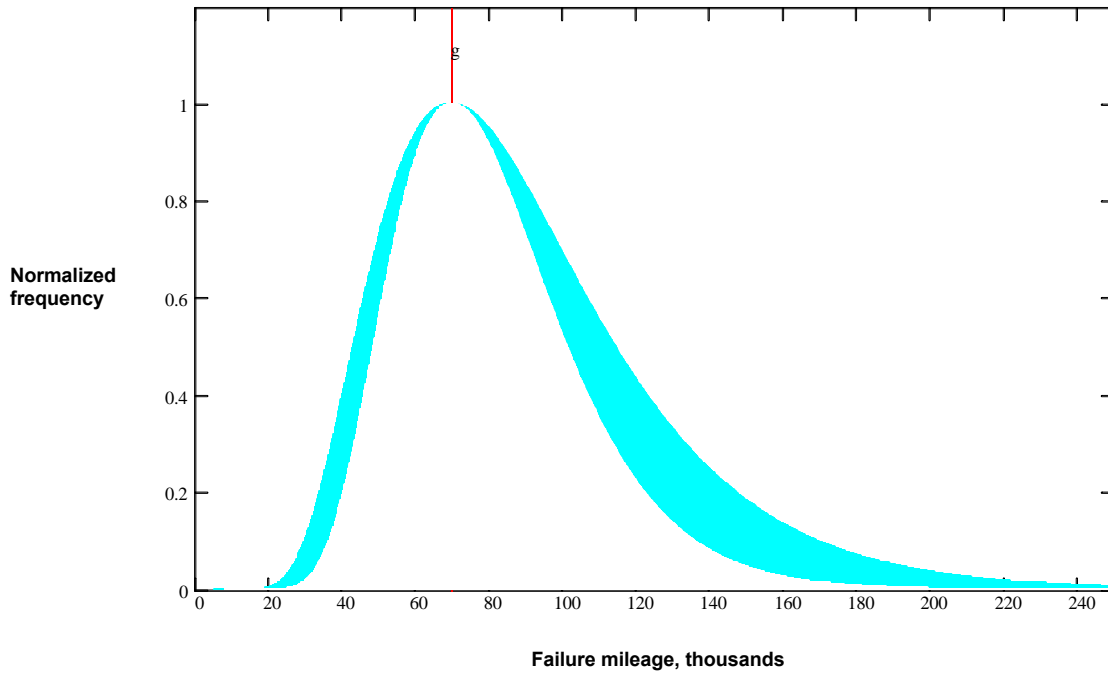


Figure 8. The band of camshaft sprocket failures calculated by Method 1: Upper bound: a span of 6 standard deviations between limiting gear tooth stress values was assumed; Lower bound: a span of 8 standard deviations between limiting gear tooth stress values was assumed. The most probable failure value, g, is 69,843 miles. See Table 2 for other parameters.

Method 2: Lobe torque model.

Upper and lower sprocket gear tooth stress limits can also be estimated if the maximum applied lobe torque and the limits of tubing expansion are known. We approach the problem of applied torque by calculating both the applied valve spring force at each point on the surface of the cam lobe and the vector of the lobe lift as a function of camshaft rotation angle. The lobe torque vector, τ , is given by

$$\tau = f \times \rho , \quad (23)$$

or in magnitude terms by

$$|\tau| = |f| \cdot |\rho| \cdot \sin(\theta) , \quad (24)$$

where f is the force applied by the valve spring at the bearing point, ρ is the distance from the center of the lobe base circle the bearing point of the cam follower, and θ is the included angle between the lobe surface normal and the radius to the lobe bearing point.

An estimate of applied torque.

A sectioned cam lobe from a 3.4L DOHC V8 SHO engine is shown in Fig. 9. This figure was scanned and digitized to produce x,y,z data which were then enhanced and converted to a lift profile using calibration data for the exhaust cam lobe [34] and a program written for this purpose [35].

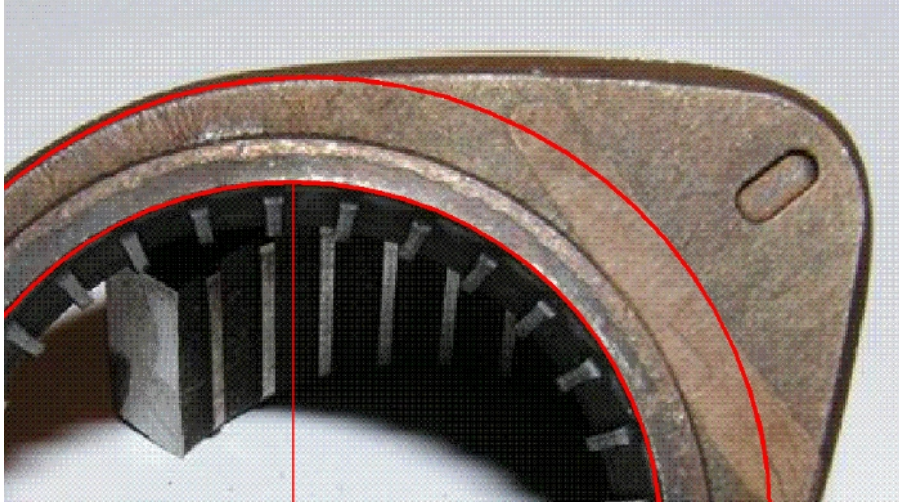


Figure 9. A sectioned Gen III SHO cam lobe. The outer circle shows the lobe base while the inner circle shows the spline base. Image enhancement techniques were used to extract the lift profile. Unmarked photo by Bob Gervais. Downloaded with permission from [2].

A polar plot of the cam lobe is shown in Fig. 10, and a standard lift profile is shown in Fig. 11. A spring constant of 146.87 pounds/inch was calculated from valve spring compression data [34] and was subsequently used by the program [35] to generate the cam lobe torque curve shown in Fig. 12. A maximum applied torque of 4.688 N-m (41.49 inch-pounds) at zero revolution rate was estimated from the program.

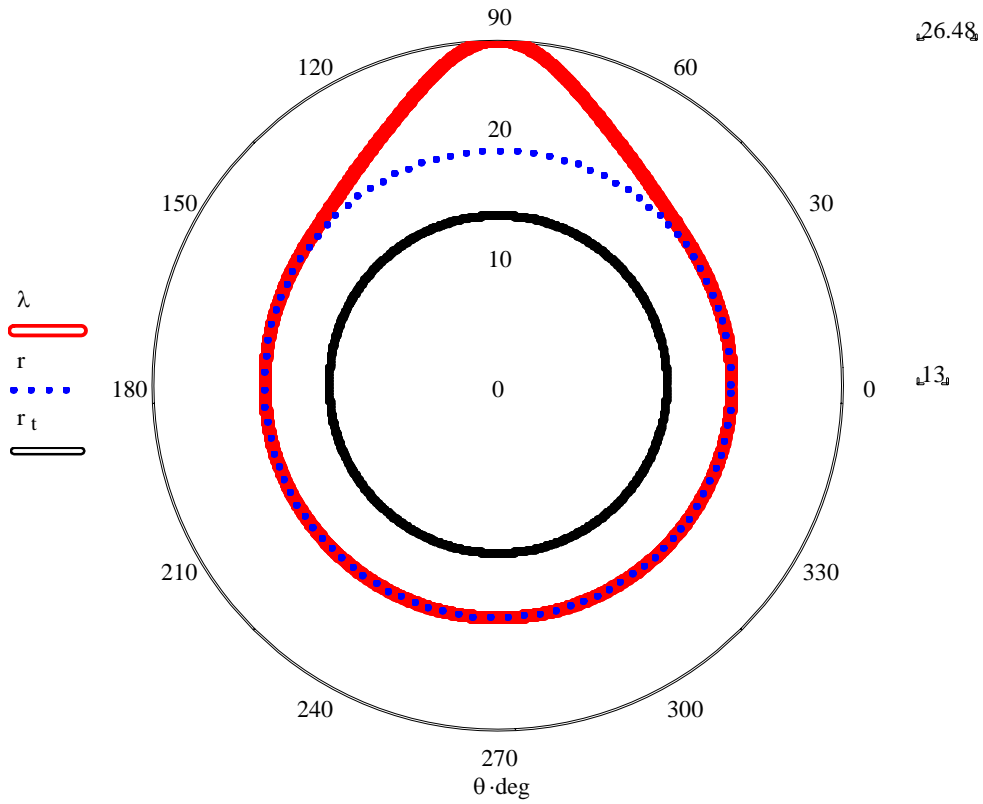


Figure 10. Polar plot of cam lobe from data digitized from [2] and calibrated according to [34]. All radial dimensions are given in mm. The lobe radius λ is given in red. The base radius r is shown as dotted blue and the tube radius r_t is shown in black.

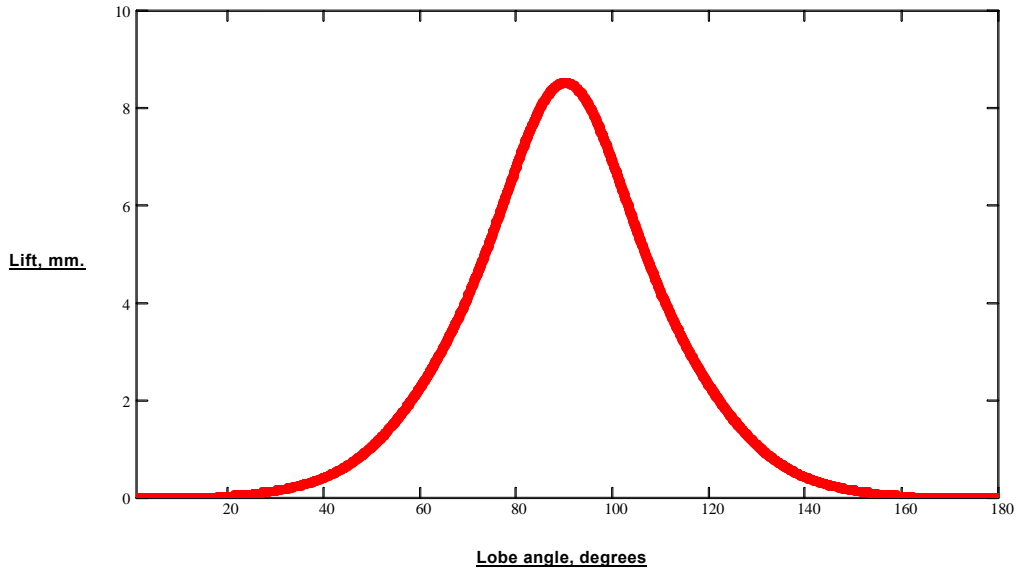


Figure 11. A standard lobe lift plot generated from the data of Fig. 7.

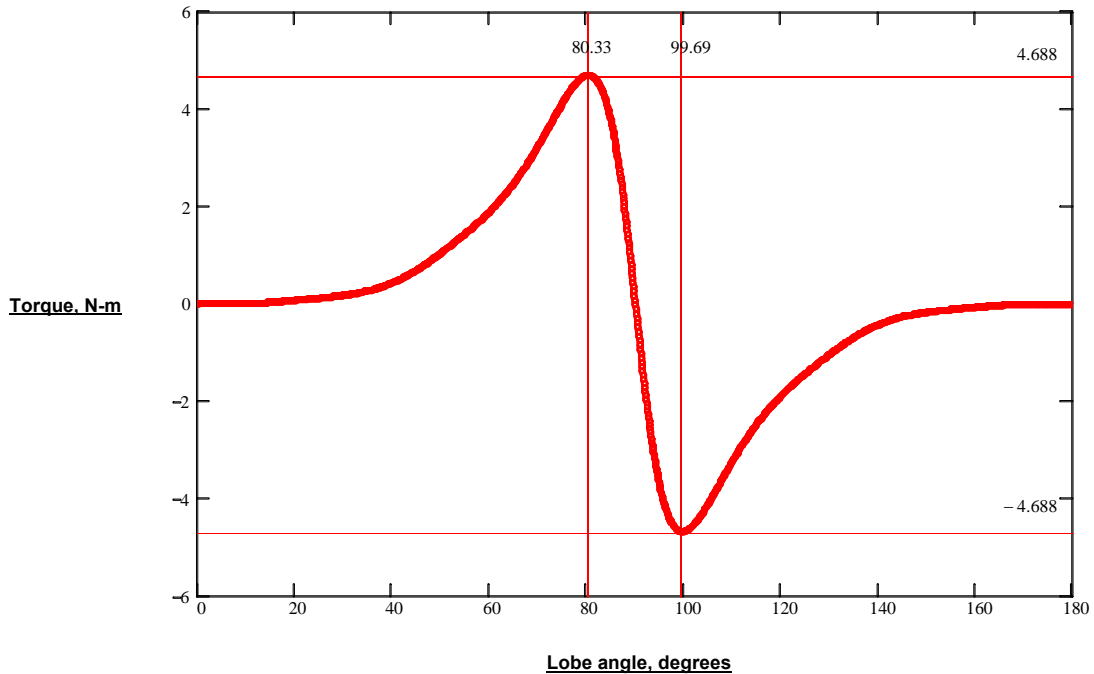


Figure 12. An estimate of the torque applied by the cam-follower system at zero rpm for each lobe rotation. Due to resonance contributions (see text below), the actual estimates are expected to be up to about 10% greater than the values shown.

The relation of specific energy to applied torque.

The work, W , done on the material is, in magnitude terms,

$$W \equiv f \cdot (w), \quad (25)$$

where w is the distance through which the force is applied. Equation 25 is equivalent to

$$W \equiv U \cdot V, \quad (26)$$

where V is the sample volume subject to stress and U is the specific energy of the material. The specific energy can be obtained by integrating the stress-strain curve:

$$U(\varepsilon) = \int \sigma(\varepsilon) d\varepsilon \quad (27)$$

Fig. 13 shows the result.

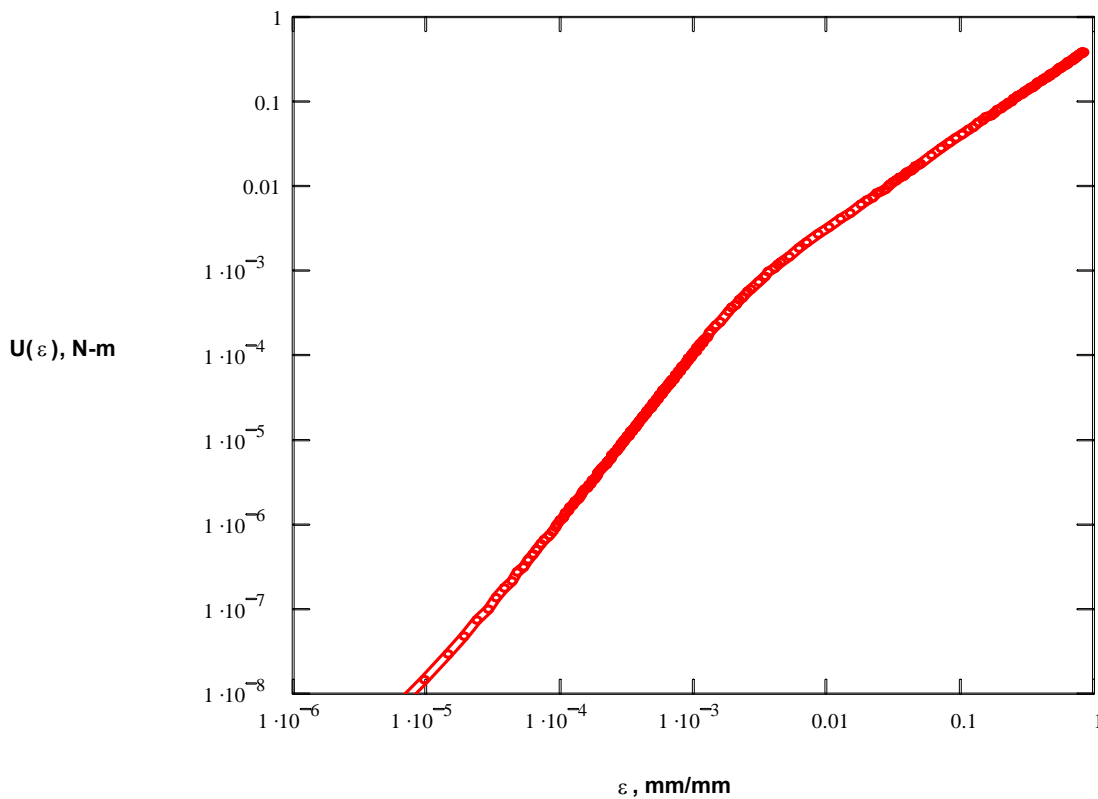


Figure 13. Specific energy as a function of strain for St52 steel (logarithmic axes). The left branch of the curve represents the elastic region of the material.

In the elastic region, $U(\varepsilon)$ simplifies to

$$U = \frac{\varepsilon^2 \cdot E}{2} \quad (28)$$

Under mandrel or hydraulic treatment, the element spline regions are compressed while plastic flow causes expansion into the element groove regions. The sample volume after mandrel expansion is presumed to be unchanged. Therefore, the volume subject to stress is

$$V = \pi \cdot d \cdot (r_o^2 - r_i^2), \quad (29)$$

where r_o and r_i are the outer and inner tubing radii, respectively, and d represents the sprocket depth as previously. Variations in tubing volume are, however, known to occur. As also noted in Method 1, a typical OD specification is 26.00 ± 0.08 mm [30,31]. This variation can determine, to a first order, the estimated lifetime of a camshaft drive sprocket.

If we now recall the torque expression, eq. 24, and write it in magnitude terms for normal force incidence, we have simply

$$\tau = f \cdot (r) \quad (30)$$

Substitution of eqs. 25 and 26 into eq. 29 yields

$$\tau = U \cdot V \cdot \frac{r}{w} \quad (31)$$

Furthermore, the material strain ε in our tubing can be written as

$$\varepsilon = \frac{w}{l}, \quad (32)$$

where

$$l = 2 \cdot \pi \cdot (r) \quad (33)$$

Consequently, after substitution of eqs. 31 and 32 into eq. 30, we have

$$\tau = \frac{U \cdot V}{2 \cdot \pi \cdot \varepsilon} \quad (34)$$

Substitution of eqs. 28 and 29 into eq. 34 gives (after conversion to N-m) the useful result

$$\tau = \frac{\varepsilon \cdot E \cdot d}{4 \cdot 10^3} \cdot (r_o^2 - r_i^2) \quad , \quad (35)$$

which can be related to failure mileage via strain-life curves in a manner similar to that given in Method 1.

Consideration of valve spring resonance forces.

In any engine using cams, the cam-follower system is subject to both forced and damped oscillations. The Ford Gen III SHO engine has a direct cam-to-valve configuration (no rocker arms) where the viscous damping is minimized. Norton [36] has adapted the solution of the forced damped harmonic oscillator (see also early references such as Synge and Griffith [37] for an alternative development of this solution) for cam-follower systems where the valve mass and spring constant are known. The solution for the valve lift α is

$$\alpha = \sqrt{\frac{1 + \left(2 \cdot \zeta \cdot \frac{\omega}{\omega_0}\right)^2}{\left[1 - \left(\frac{\omega}{\omega_0}\right)^2\right]^2 + \left(2 \cdot \zeta \cdot \frac{\omega}{\omega_0}\right)^2}} \quad , \quad (36)$$

where

$$\zeta = \frac{\gamma}{2 \cdot m \cdot \omega_0} \quad ,$$

and

$$\omega_0 = \sqrt{\frac{k}{m}} \quad ,$$

where

- ω = system frequency,
- γ = damping constant,
- k = spring constant, and
- m = valve mass.

As the system frequency approaches full resonance, additional force is placed on the valve spring and consequently additional peak torque is placed on the lobe. Catastrophic resonance occurs when the rotational frequency closely approaches the natural frequency of the cam-to-valve system. In most modern engine designs, however, the rotational

speeds are held well below peak resonance frequency. A design rule [36] for modern engines is that engine rotational speeds should be held sufficiently below resonance frequency so that only about 110% of the base applied spring force is achieved at maximum operational rotation speed. By design, the maximum rotation speed is consequently only about 33% of the rotation speed at maximum resonance force. Fig. 11 shows an estimate of the peak lobe torque (proportional to valve lift) for the Ford Gen III SHO engine as a function of engine speed.

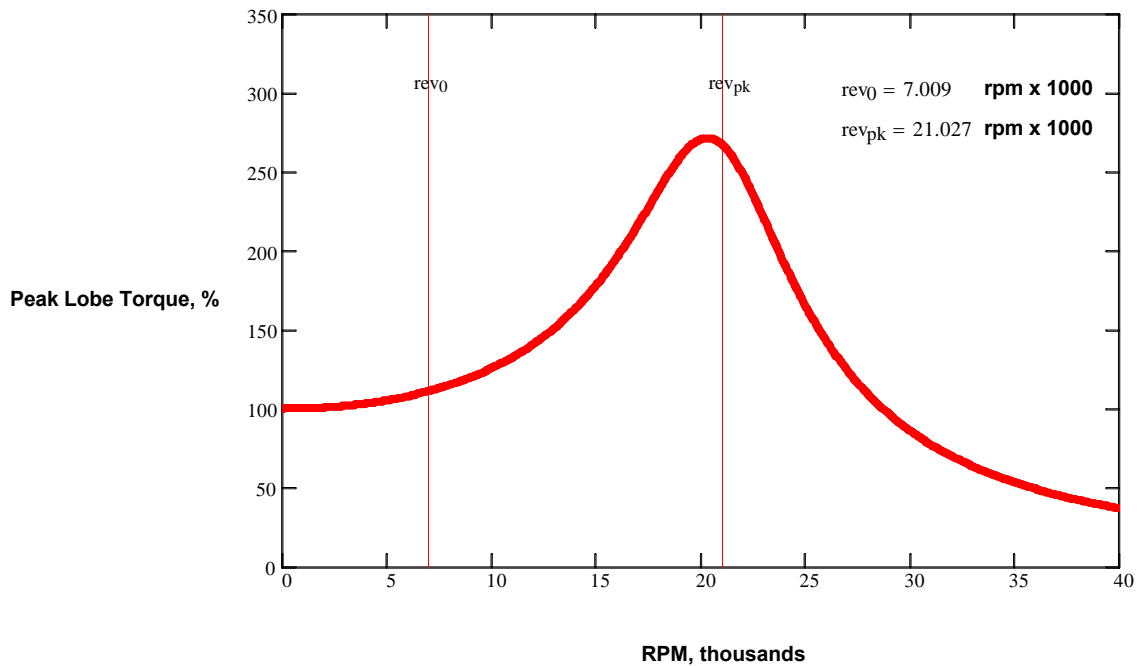


Figure 11. Estimated peak lobe torque as a function of crankshaft rotation speed. Assumed values were: $m = 21.22$ gram (1.212×10^{-4} blob [36]), $k = 25.72$ N/mm (146.87 lb/in), and $\gamma = 0.05$.

In order to establish some most probable and limiting values of sprocket lifetime, the peak lobe torques corresponding to values within the design resonance interval were calculated for three cases of assumed engine service: (1) a limiting case at zero RPM which represents the minimum peak lobe torque that can possibly be applied; (2) a relatively conservative case typified by constant open interstate driving at approximately 75 mph (cruise conditions) in 4th (top) gear; and (3) absurdly aggressive driving indicated by running the engine constantly at redline (equivalent to approximately 90 mph in 2nd gear). The torque values thus calculated are reported in Table 3 below.

Table 3. Peak lobe torque values calculated according to designed valve lift resonance (see Fig. 11) and other variables associated with various driving styles encountered with the Ford Gen III SHO.

Driving Style	Immobile	Conservative	Aggressive
Crankshaft RPM	0	2655	7009 (redline)
Resonance Force	100%	101.5%	111%
Speed, MPH	0	75.4	89.5
Transmission Gear	4 th	4 th	2 nd
Torque, N-m	4.688	4.759	5.224

Using eq. 35 and typical supplier variations in tubing OD, a set of torque-mileage curves can be calculated. The intersection of the torque lines from Table 3 with the torque-mileage curves provides estimates of the limits of failure mileage for one cam lobe. Fig. 12 shows the result.

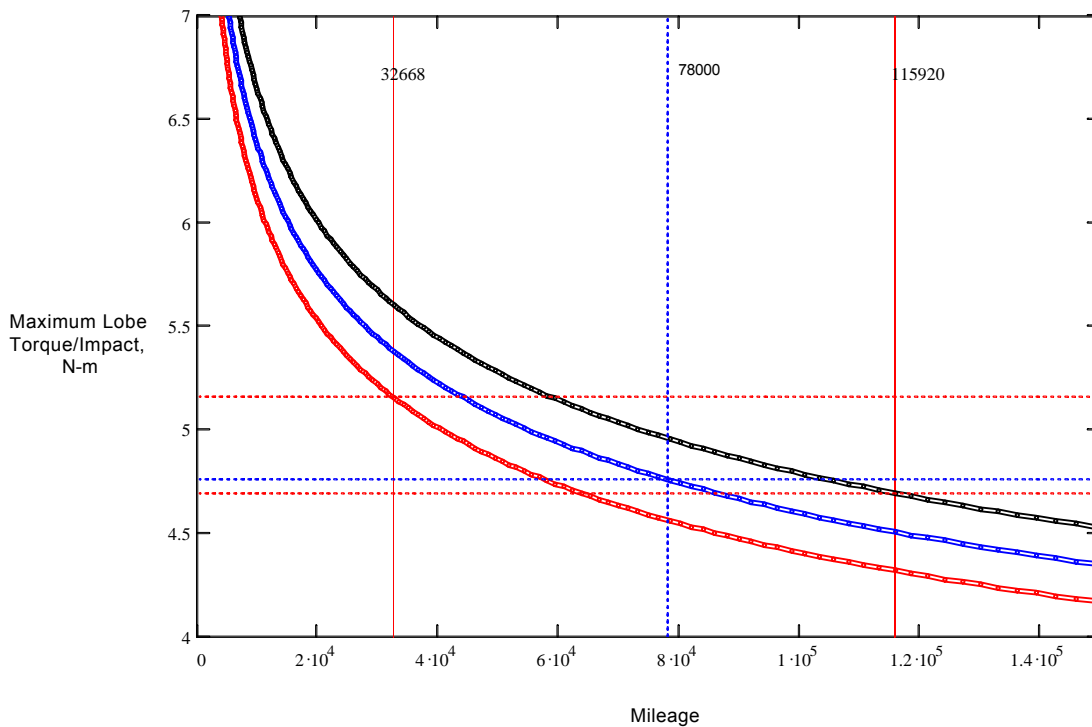


Figure 12. Torque-mileage curves for various OD St52 DOM tubing having an ID of 25 mm. Red: 25.92 mm; Blue: 26.00 mm; and Black: 26.08 mm.

While a range of failure mileages is apparent for a single lobe of known peak torque, the drive sprocket actually counters the torque of all eight lobes on each camshaft. This means that the drive sprocket is subject to eight times the number of stresses that each lobe endures. Mathematically, if all eight lobes are equivalent, the net effect is to multiply the standard deviation of the lobe failure distribution by $(8)^{1/2}$ [26, 38]. This means that the form of the Birnbaum-Saunders equation (eq. 6) becomes

$$\phi_{\text{sprocket}} = \frac{1}{2 \cdot (\sqrt{8}) \cdot \sqrt{2 \cdot \pi} \cdot c \cdot \mu} \cdot \left[\left(\frac{n}{\mu} \right)^{\frac{-1}{2}} + \left(\frac{n}{\mu} \right)^{\frac{-3}{2}} \right] \cdot \exp \left[\frac{-1}{2 \cdot (8) \cdot c^2} \cdot \left[\left(\frac{n}{\mu} \right)^{\frac{1}{2}} - \left(\frac{n}{\mu} \right)^{\frac{-1}{2}} \right]^2 \right] \quad (36)$$

In a manner similar to that shown in Method 1, a band of failure can also be calculated using eq. 36. The constants used are derived from Fig. 12 and are given in Tables 4 and 5.

Table 4. Values of r_o , τ (from Fig. 12), and failure mileage used to estimate the span of the failure distribution.

<u>Position</u>	<u>r_o, mm</u>	<u>τ, N-m</u>	<u>Mileage</u>
Low	25.92	5.224	32,668
most probable	26	4.759	78,000
High	26.08	4.688	115,920

Table 5. Birnbaum-Saunders constants for eq. 36

<u>Span, std dev</u>	<u>c</u>	<u>μ, miles</u>
6	0.149	79,757
8	0.112	78,984

The graphical results are given in Fig. 13.

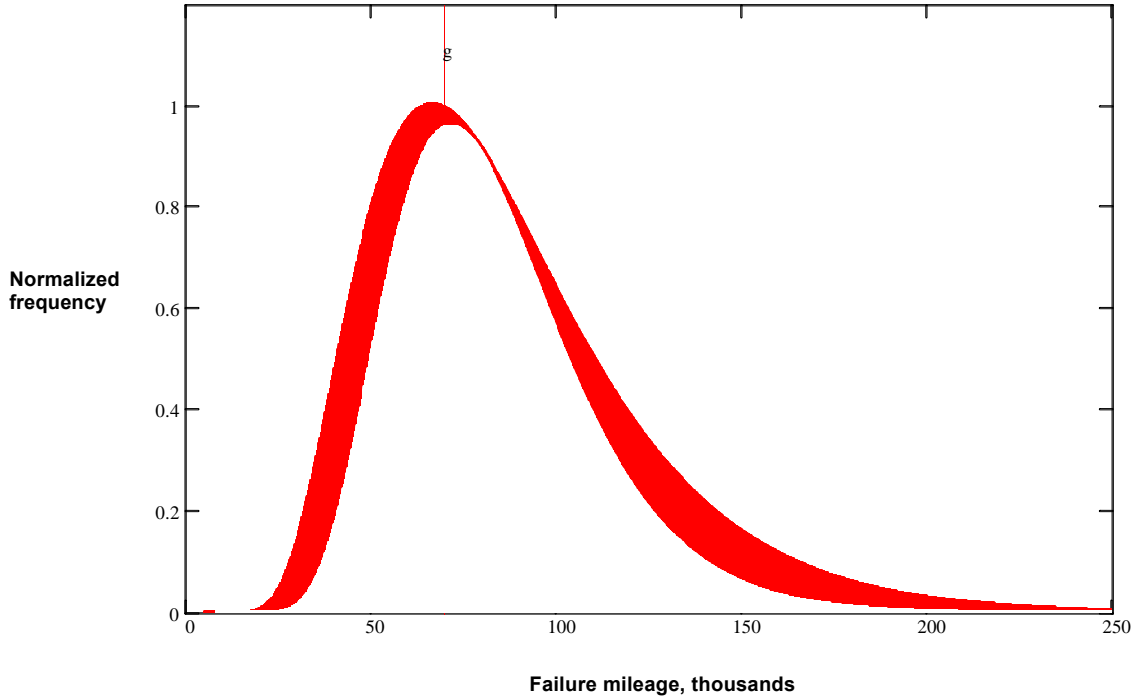


Figure 13. The band of camshaft sprocket failures estimated by Method 2 (eq. 36): Upper bound: a span of 6 standard deviations between limiting peak lobe torque values was assumed; Lower bound: a span of 8 standard deviations between limiting peak lobe torque values was assumed. The most probable failure value, g , calculated by Method 1, is shown for comparison. See Tables 4 and 5 for other parameters.

This method does have the distinct advantage that the assumption of a gear tooth stress limit (as in Method 1, eq. 13) is not required. Calculation of a failure band very similar to that produced by Method 1 does, however, support the validity of the criterion of the gear tooth stress limit. A disadvantage of this method is that an accurate lobe lift profile is required.

Analysis of the Failure Data.

The publicly reported camshaft failure mileage data are sufficient in sample size to produce better than a 95% confidence level [39]. We chose to analyze this sample by first fitting a Birnbaum-Saunders equation to the cumulative data using a non-linear least squares technique in a program written for this purpose [40]. A residual plot (not shown) did not show any systematic deviation from the fitting scheme (for an example of the use of residual plots, see [41]). We found an average deviation of the fit from the data of less than 4% and Chi-square significance at the 95% and 99% confidence levels. This procedure also yields the median and shape parameters which can subsequently be used to calculate the derivative (pdf) equation for direct comparison with both binned data and the physical models previously described. A Fourier transform of the data [3] did not yield evidence of multiple components above the sample noise. The data appear, then, to

be typical of one predominant manufacturing event (most likely using several camshaft assembly machines in parallel) and do not suggest large multiple production runs with significantly different medians and variances. We cannot, however, rule out the possibility of a partial or whole production run that failed and was corrected before the expiration of the 36,000 mile warranty. A small number of failures before the warranty expiration mileage have been reported. These may be due to extremely low annual mileage rates such that the warranty time of 36 months had expired. The cumulative data, the fitted Birnbaum-Saunders cdf, and the calculated fit constants are shown in Fig. 14. The fitted pdf is also shown against binned data in Fig. 15.

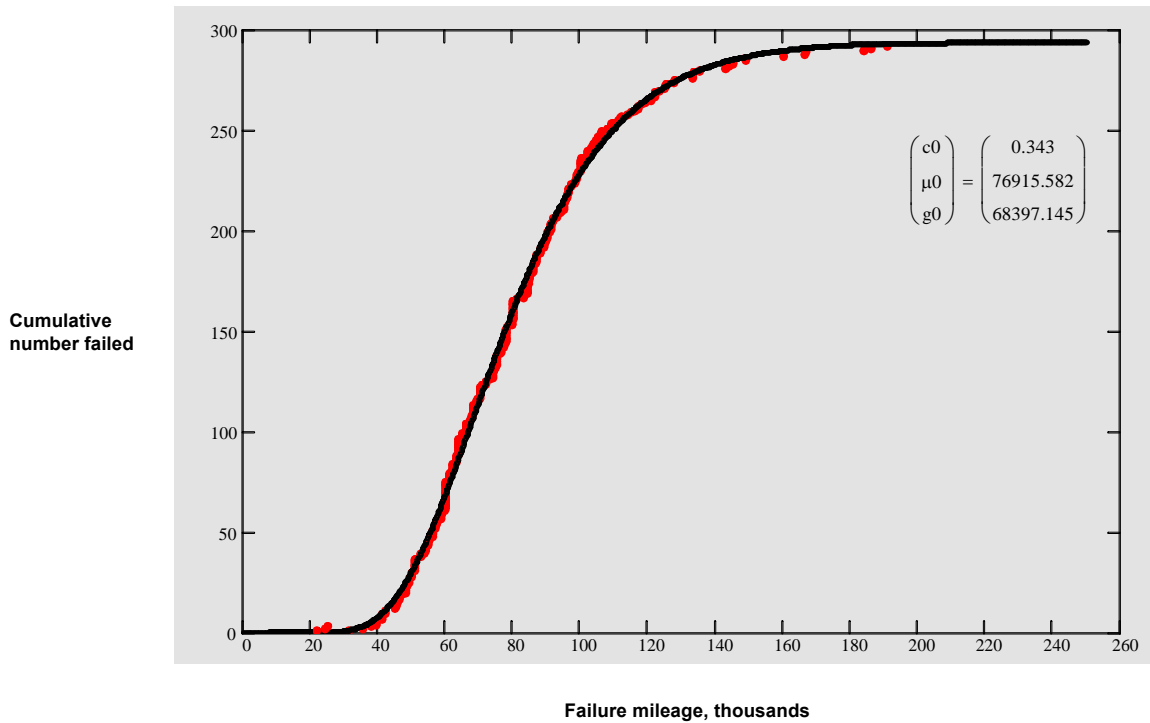


Figure 14. Cumulative camshaft drive sprocket failures as a function of miles driven. Red dots: Reported failures as of April 2004; Black line: Non-linear least squares fit of a simple Birnbaum-Saunders distribution cdf having the form of eq. 5. The values of the fit constants are shown in the upper right corner of the figure.

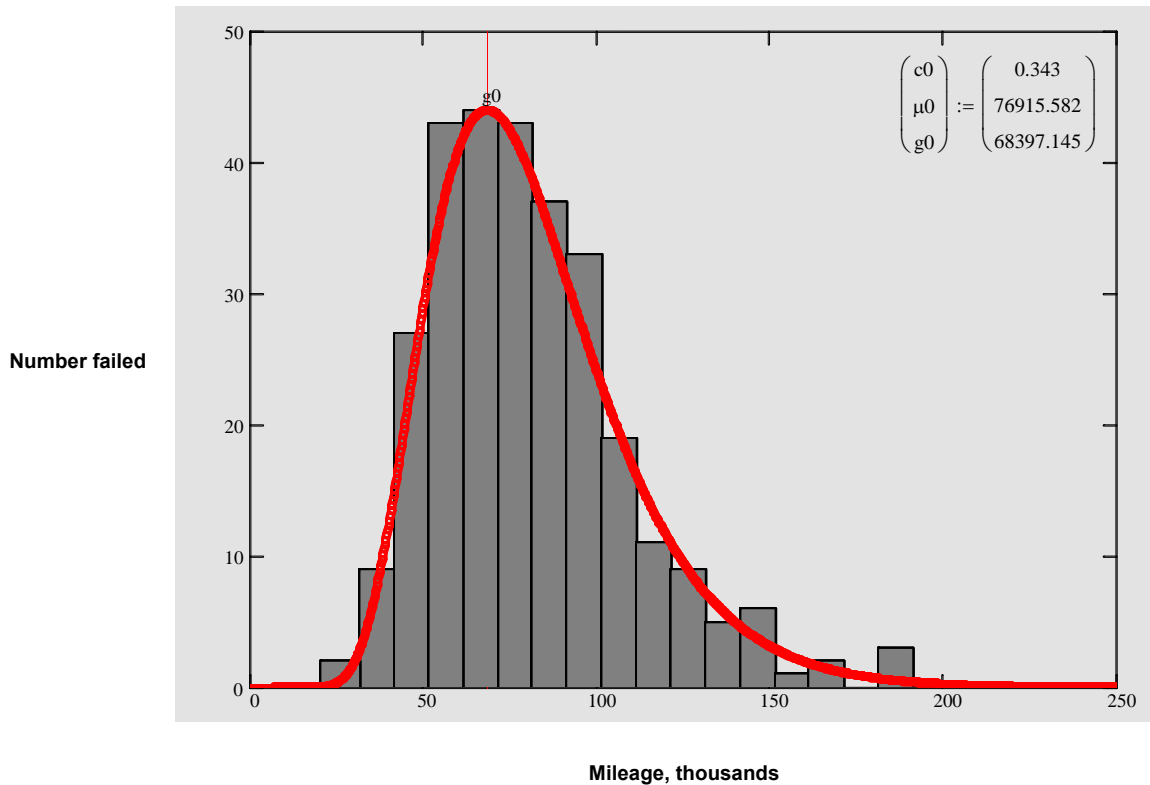


Figure 15. Comparison of binned failure data (grey bars) with a simple Birnbaum-Saunders pdf having the form of eq. 6 (red line). The bin interval was approximately 10,000 miles [40]. The fit constants shown are the same as those of Fig. 14.

RESULTS AND DISCUSSION

Comparison with Failure Models.

Figure 16 shows the curve of the pdf fitted from the failure plotted on the background of the failure bands predicted by Method 1 and Figure 17 shows an analogous comparison to the failure band derived from Method 2.

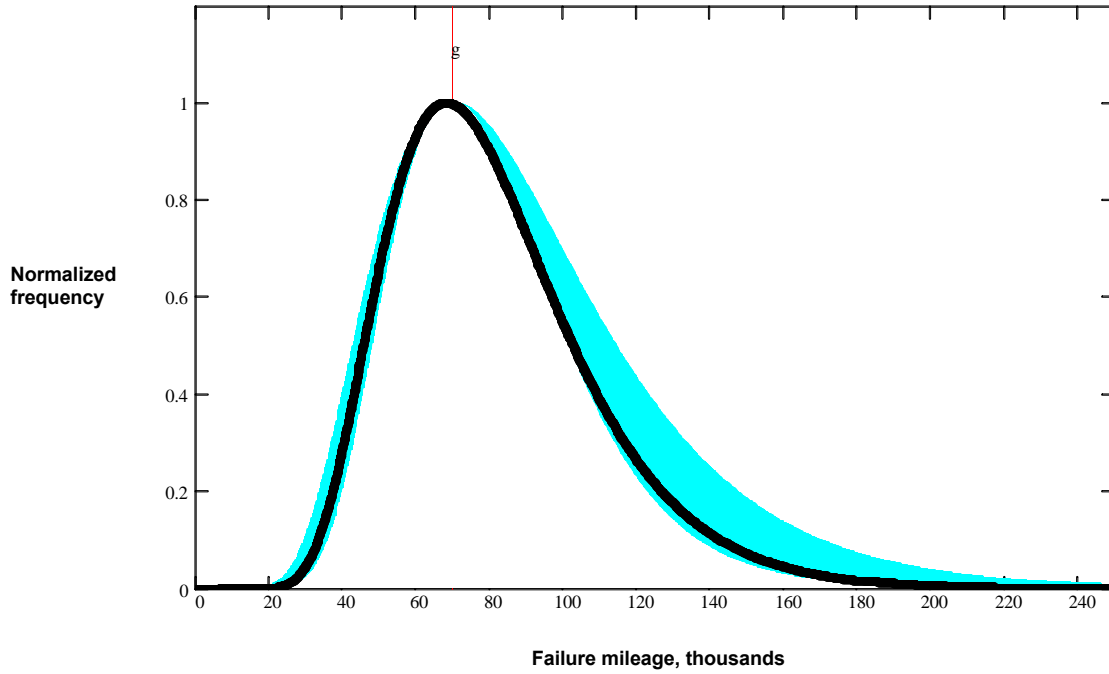


Figure 16. Comparison of the sprocket failure band (cyan) calculated by Method 1 with the fitted pdf (from Fig. 15) of the failure data (black).

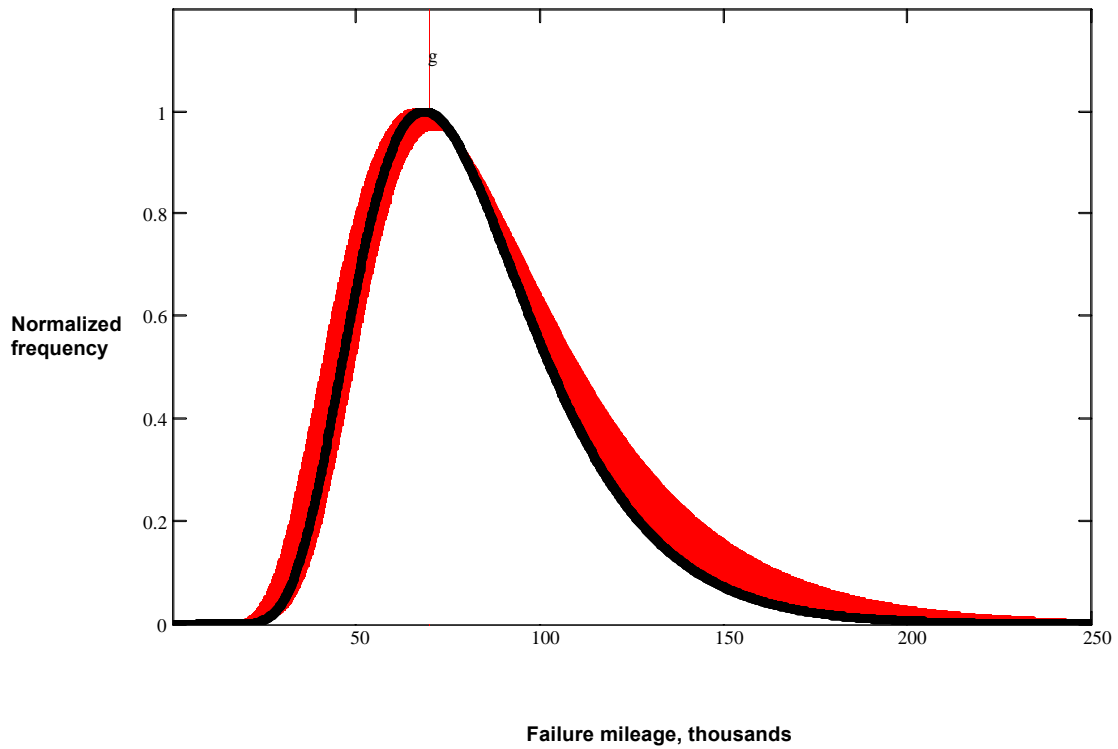


Figure 17. Comparison of the sprocket failure band (red) calculated by Method 2 with the fitted pdf of the actual failure data (black).

By either model method, the fitted pdf function of the failure data lies almost entirely within the error bands predicted. Apparently, camshaft sprocket failures can be well predicted from general physical principles and the assumption of either a gear tooth stress limit or a design rule of valve train resonance, either of which were well known before Ford Gen III SHO engine production commenced.

A Vulnerability Estimate.

Either the models (Method 1 or Method 2) or the fitted failure function of Fig. 14 can be used further to estimate the vulnerability of the entire lot of Ford Gen III SHO vehicles to camshaft sprocket failure if the mean yearly mileage is known. The Office of Transportation Technologies has estimated the mean yearly automobile miles driven at 11,988 [45]. We have used that value and the fitted cdf of Fig. 14 to extract the fraction of vehicles subject to failure for the mean estimated mileage driven for each model year. Furthermore, the resulting vulnerability (mean aggregate % subject to fail) reported in Table 5 can only be expected to increase with the further passage of time.

Table 5. Mean vulnerability estimate (number and percentage) of camshaft sprocket failures for Ford Gen III SHO vehicles (before camshaft repair and preventive maintenance).

	Total				
Model Year	1996	1997	1998	1999	
Mean miles driven as of 6/2004	101898	89910	77922	65934	
Mean yrs driven as of 6/2004	8.5	7.5	6.5	5.5	
% Subject to fail	79.5	67.7	51.6	32.7	
# Vehicles made [2]	5033	10133	2317	2247	19730
# Subject to fail	4001	6860	1196	735	12792
Mean aggregate % Subject to fail					64.8

Methods to Extend Drive Sprocket Life.

Methods for extending the life of the camshaft drive sprocket were also discussed in the patent literature of the time [15,44]. Reduction of stress on the drive sprocket can be accomplished by crimping, dimpling, adhesive bonding, brazing, and welding [42]. Methods for pinning the drive sprocket have also been reported [43,44]. Using the predictive methods given above, estimates of camshaft drive sprocket life after redesign for stress reduction can also be made.

One remedy for stress reduction would have been merely to extend the depth (thickness) of the drive sprocket in the original design. While this method would not permit convenient retrofits on existing Ford Gen III SHO camshafts, we offer the calculations for completeness. If the depth, d , of the drive sprocket were elongated 50% from 15.24

mm to 22.86 mm, then, according to Method 1, the most probable failure mileage increases to 1,330,800 miles, and the expected failure pdf band is as shown in Fig. 18. Also note that, under these conditions, the onset of sprocket failure is not expected to occur until approximately 500,000 miles.

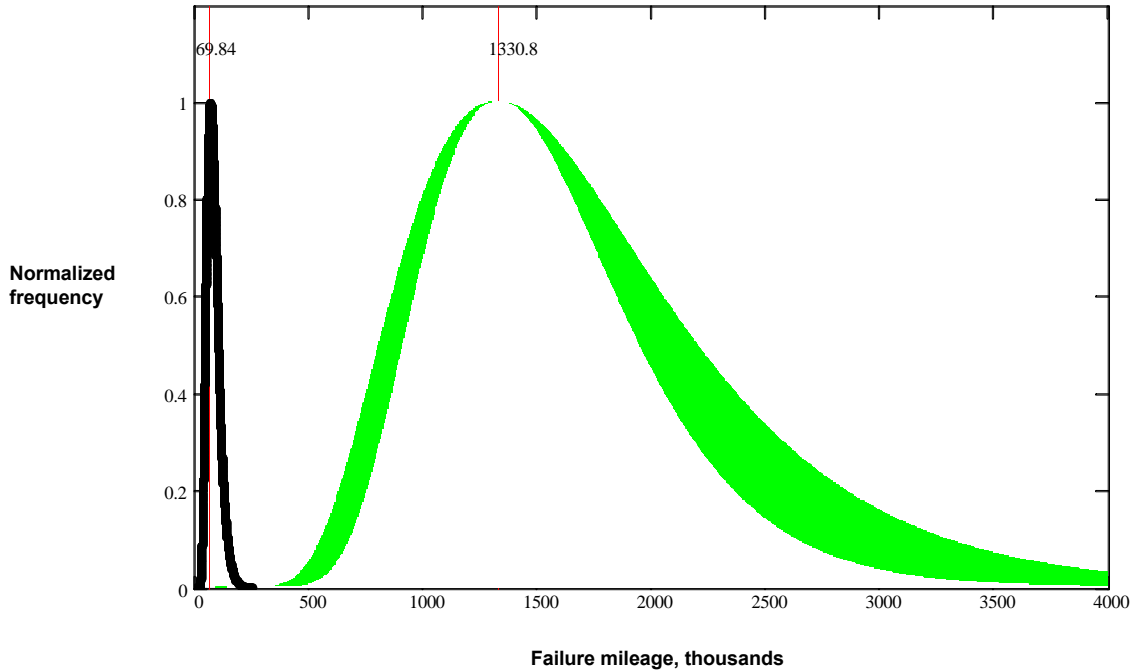


Figure 18. An estimate of the failure band (green) for a 50% increase in camshaft drive sprocket depth (thickness). The actual failure pdf (black) is also shown for comparison.

A second remedy for reduction of stress in assembled camshaft drive sprockets is welding. This is often the method of choice if clearance for other camshaft elements is an issue. Welding is a method that can add material to the stress region. If the weld material is essentially the same as St52 steel; i.e., no foreign filler rod is used, and a sufficiently clean weld process is performed (TIG or laser welding, for example), then the weld on the drive sprocket can be modeled with the lifetime methods given above. In particular, we can employ Method 1 and estimate a new contact area after welding and subsequently make a prediction of service lifetime based on the lowered sprocket stress. It is well known that Young's modulus changes only minimally under such weld conditions; and so our values are unchanged for the purposes of prediction. If, for instance, three welds each of size sufficient to produce 3 mm arc length in contact with the sprocket splines (the actual bead would be considerably longer since the spline occupies less arc length than the groove) and 3 mm width are placed symmetrically around the sprocket and bond to both the sprocket and the tubing, then Method 1 estimates a lifetime as shown in Fig. 19. The parameters used are given in Table 6. The

onset of failures is estimated at beyond 500,000 miles, and the most probable failures are expected at about 1.5 million miles.

Table 6. Values of δr , σ , and failure mileage for three symmetrically placed welds each of 3 mm arc length and 3 mm width. The lifetime was subsequently estimated by Method 1.

<u>Position</u>	<u>δr, microns</u>	<u>σ, MPa, after weld</u>	<u>Mileage</u>
low	96	73.30	731,340
most probable	112.5	66.28	1,528,000
high	156	52.92	8,019,000

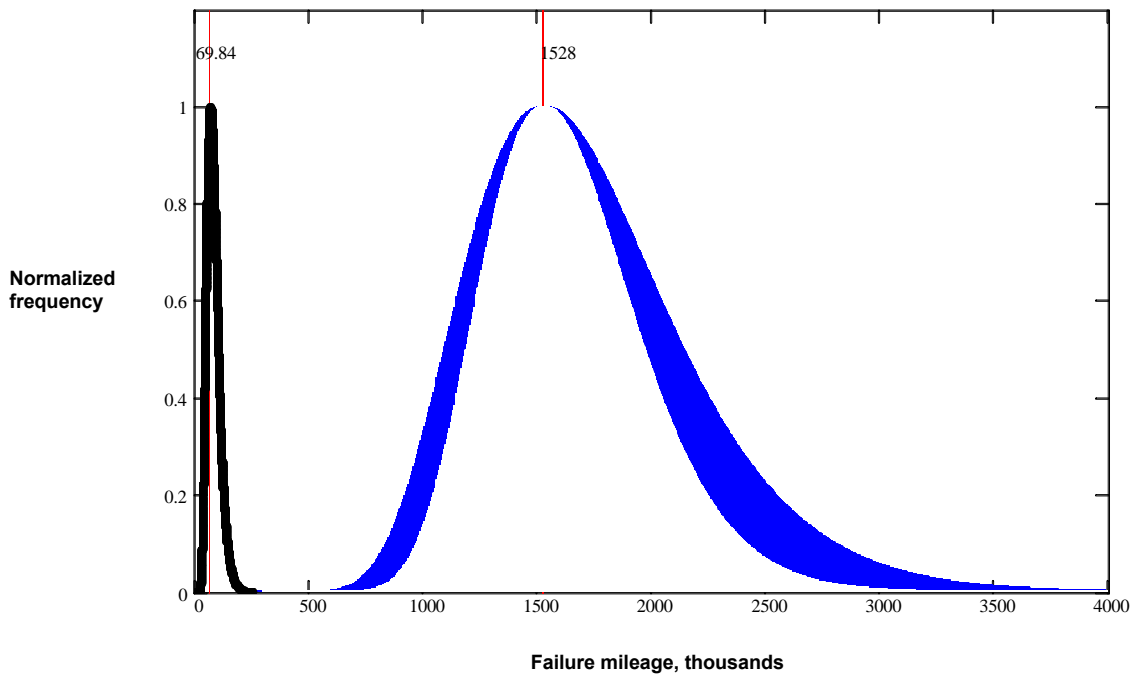


Figure 19. An estimate of the failure band (blue) if the drive sprocket were welded to the tubing with three beads sized and placed as described in the text above. The actual failure pdf (black) is also shown for comparison.

CONCLUSIONS AND RECOMMENDATIONS

We have demonstrated that the engineering, mathematics, and patent literature of the time before production of the Ford Gen III SHO engines should have enabled any engineer competent in this field to determine that the assembled camshafts in those engines would experience premature failure at the mileages later actually observed. Furthermore, remedies (such as welding) could have been implemented prior to production. On the basis of the results given in this paper, the following questions for legal discovery are recommended:

1. Was Thyssen-Krupp Presta in fact the supplier of the Ford Gen III SHO camshafts?
2. What camshaft specifications did the supplier provide to Ford Motor Co.?
3. What was the species and grade of steel actually used in the Ford Gen III SHO camshafts?
4. What was the OD runout tolerance of the tubing used?
5. Did Ford Motor Co. perform any lifetime estimates of these camshafts based on the supplied materials and dimensions before production? If so, what were the results?
6. Did Ford Motor Co. perform any destructive testing of these camshafts in engines before production began?
7. Did Ford Motor Co. perform any destructive testing of Gen III SHO camshafts with welded drive sprockets? If so, what were the results?
8. According to Ford Motor Co. records, what percentage of the total Ford Gen III SHO production has experienced camshaft failure?
9. Before production, what was the cost estimate to (a) increase the drive sprocket depth; or (b) weld the drive sprocket after assembly?
10. Does Ford Motor Co. or its supplier(s) have internal company data that supports or refutes the assertions of this paper?

ACKNOWLEDGMENT

The author wishes to thank Dr. Robert Hermes of Los Alamos National Laboratory for a critical reading of this manuscript and useful discussions.

REFERENCES

1. Case number 02-CH-22086 was filed on 12/10/02 in the Circuit Court of Cook County Illinois, County Department, Chancery Division. The complainants are Larry Eck, of Wheaton, IL, and Timothy Wright, of Decatur, IL. On behalf of their clients, the law firm of Edelman, Combs & Latturmer, LLC (www.edcombs.com) filed a three-count complaint against Ford Motor Company. All three counts center on consumer fraud. It will seek to identify a class of parties that have been/will be injured as a result of this alleged fraud.
2. <http://www.V8sho.com/>
3. Engineering Statistics Handbook, NIST, <http://www.itl.nist.gov/div898/handbook/eda/section1/eda1.htm>
4. Begley, S., “Ban on ‘Junk Science’ Also Keeps Jurors From Sound Evidence”, Wall Street Journal, June 27, 2003, B1
5. Leaney, P.G., and Marshall, R., http://www.lboro.ac.uk/departments/mm/research/product-realisation/res_int/ipps/docs/autoch3.pdf, p. 20.
6. Schagrin, R.B., <http://www.ustr.gov/sectors/industry/steel201/Responses/ER-079-Revised%20CPTI%20Exclusion%20Responses.pdf>, “Re: Revised Public Comments on Potential Action Under Section 203 of the Trade Act of 1974 With Regards to Imports of Certain Steel: Domestic Producers’ Response to Requests to Exclude Products From Import Relief”, Jan 22, 2002, p.5.
7. Boller, C., and Seeger, T., Materials Data for Cyclic Loading, Part A: Unalloyed Steels, Elsevier, New York, 1987, pp 158-168.
8. Comer, J., http://www.me.iastate.edu/me515_comer/Lecture/lecture22.pdf and [/lecture25.pdf](http://www.me.iastate.edu/me515_comer/Lecture/lecture25.pdf).
9. Lamartine, B., St52BollerSeeger2.mcd, a Mathcad program to fit and plot four parameter strain-life equations, July 30, 2004, unpublished.
10. Ilzhofer, B., et al., “Shape Optimization Based on Parameters from Lifetime Prediction”, NAFEMS Seminar: Fatigue Analysis, Wiesbaden, Germany, November 8-9, 2000.
11. Breuer, H-J., et al., “Process for Producing an Assembled Camshaft as well as Assembled Camshaft Consisting of a Shaft Tube and Slid-On Elements”, U.S. Patent # 5,101,554, issued April 7, 1992.

12. Swars, H., and Grewe, H., "Process for Allowing Pretreatment of Assembled Camshaft Components", U.S. Patent # 5,037,490, issued August 6, 1991.
13. Bendoraitas, J., and Clark, J., "Camshaft Manufacture", U.S. Patent # 4,809,562, issued Mar 7, 1989.
14. Bendoraitas, J., and Clark, J., "Camshaft Manufacture", U.S. Patent # 4,847,963, issued July 18, 1989. This issue was based on a divisional application from [13].
15. Arnold, P., and Kaywood, R., "Tubular Camshaft Assemblies and the Like", U.S. Patent # 4,922,785, issued May 8, 1990.
16. Arnold, P., and Kaywood, R., "Apparatus for Making Tubular Camshaft Assemblies", U.S. Patent #4,841,627, issued June 27, 1989.
17. Van Vlack, L., Elements of Materials Science, Addison-Wesley, Reading, Massachusetts, 1959, pp. 330-332.
18. Lamartine, B., Forcelock.mcd, a Mathcad program modeling force-locking expansion in DOM tubing, June 9, 2004, unpublished.
19. Massa, E., Costruzione di macchine. Editori Masson Italia, Milano, 1981.
20. GE Product Design,
http://geplastics.com/resins/global/pdf/design_guides/productdesignsec4.pdf
21. Purdue University posted materials science lectures,
<http://pasture.ecn.purdue.edu/~abc330/gear2.pdf>
22. Thor, cited in Rigberth, J., "Simplified Design of Fire Exposed Concrete Beams and Columns", <http://www.brand.lth.se/bibl/5063.pdf>
23. "Fatigue Theory", Chapter 13,
http://hpc.snu.ac.kr/document/patran2001r2/patran2001r2/helpfiles/pdf_patran/add_ons/fatigue/fat_theory.pdf
24. Birnbaum, Z., and Saunders, S., "A New Family of Life Distributions, Journal of Applied Probability, 6 319 (1969).
25. Engineering Statistics Handbook, NIST,
<http://www.itl.nist.gov/div898/handbook/apr/section1/apr166.htm>
26. Apostol, T., Calculus, Vol. II: Calculus of Several Variables with Applications to Probability and Vector Analysis, Blaisdell, New York, 1962, pp. 152-154.

27. Kawamura, T., and Iwase, K., “Characterizations of the Distributions of Power Inverse Gaussian and Others Based on the Entropy Maximization Principle”, J. Japan Statist. Soc., 33 (1) 95 (2003).
28. Ng, H.K.T., et al., “Modified Moment Estimation for the Two-Parameter Birnbaum-Saunders Distribution”, Computational Statistics & Data Analysis, 43 283 (2003).
29. <http://v8sho.com/SHO/caranddriver2.html>
30. H J Garay Co., http://www.hjgaray.es/ingles/tribos/tubNomen_ING.htm
31. Parker Steel International, 4239 Monroe St., Toledo Ohio, 43606-0883, <http://www.metricmetal.com>
32. Hamilton, J., “Hamilton’s Cam Shaft Disassembly”, December 19, 2003, <http://v8sho.com/SHO/HamiltonsCamShaftDisassembly.htm>
33. Usui, E., et al., “Analytical Prediction of Three-Dimensional Cutting Process, Part 3: Cutting Temperature and Crater Wear of Carbide Tool”, Journal of Engineering for Industry, 100 (5) 236 (1978).
34. Engine and Torque Specifications, <http://www.v8sho.com/allspecs.html>
35. Lamartine, B., V8sholobe2.mcd, a Mathcad program for estimating the maximum applied cam lobe torque and the lobe lift profile, April 19, 2004, unpublished.
36. Norton, R., Cam Design and Manufacturing Handbook, Industrial Press, 2002, pp. 274-279. See also other earlier editions of this well-known handbook.
37. Synge, J., and Griffith, B., Principles of Mechanics, McGraw-Hill, New York, 1959, pp. 146-153.
38. Wikipedia, The Free Encyclopedia, “Illustration of the Central Limit Theorem”, <http://en.wikipedia.org/wiki/>
39. iSixSigma, “How to Determine Sample Size”, <http://www.isixsigma.com/library/content/c0007609ex.asp>
40. Lamartine, B., Birnbaum-Saunders5new.mcd, a Mathcad program that fits raw failure data to a simple Birnbaum-Saunders distribution, March 15, 2004, unpublished.
41. Ledvij, M., Primer: “Curve Fitting Made Easy”, The Industrial Physicist, wysiwyg://3/http://www.aip.org/tip/INPHFA/vol-9/iss-2/p24.htm

42. Cox, et al., "Method for Assembling a Camshaft", U.S. Patent # 6,182,361, issued February 6, 2001.
43. The SHOSHOP, 96-'99 SHO Guidelog, Chapter 2: Performance, Roll-Pin Solution on Camshafts, <http://www.shoshop.com>
44. Mettler-Friedli, K., "Assembly of a Cylindrical Body Made to Finished Dimensions", U.S. Patent # 5,299,881, issued April 5, 1994, PCT Publication Date: February 20, 1992.
45. Office of Transportation Technologies, "Vehicle Miles of Travel (VMT) and Age by Vehicle Type", <http://www.ott.doe.gov/facts/archives/fotw227.shtml>